Article

Aryl hydrocarbon receptor is a tumor promoter in *MYCN*-amplified neuroblastoma cells through suppression of differentiation

Kanita A. Chaudhry, Justine J. Jacobi, Bryan M. Gillard, ..., Dominic J. Smiraglia, Mark D. Long, Anna Bianchi-Smiraglia

Mark.Long@RoswellPark.org (M.D.L.)
Anna.Bianchi-Smiraglia@RoswellPark.org (A.B.-S.)

Highlights

AhR is a targetable tumor promoter in *MYCN*-amplified neuroblastoma

AhR positively regulates MYCN in *MYCN*-amplified neuroblastoma cell

AhR antagonists and retinoids induce durable differentiation of neuroblastoma cells

Article

Aryl hydrocarbon receptor is a tumor promoter in *MYCN*-amplified neuroblastoma cells through suppression of differentiation

Kanita A. Chaudhry,[1] Justine J. Jacobi,[1] Bryan M. Gillard,[2] Ellen Karasik,[2] Jeffrey C. Martin,[1] Tatiane da Silva Fernandes,[1] Edward Hurley,[3] Maria Laura Feltri,[3,4] Kristopher M. Attwood,[5] Clare J. Twist,[6] Dominic J. Smiraglia,[1] Mark D. Long,[2,5,*] and Anna Bianchi-Smiraglia[1,7,*]

SUMMARY

Neuroblastoma is the most common extracranial solid tumor in children. *MYCN* amplification is detected in almost half of high-risk cases and is associated with poorly differentiated tumors, poor patient prognosis and poor response to therapy, including retinoids. We identify the aryl hydrocarbon receptor (AhR) as a transcription factor promoting the growth and suppressing the differentiation of *MYCN*-amplified neuroblastoma. A neuroblastoma specific AhR transcriptional signature reveals an inverse correlation of AhR activity with patients' outcome, suggesting AhR activity is critical for disease progression. AhR modulates chromatin structures, reducing accessibility to regions responsive to retinoic acid. Genetic and pharmacological inhibition of AhR results in induction of differentiation. Importantly, AhR antagonism with clofazimine synergizes with retinoic acid in inducing differentiation both *in vitro* and *in vivo*. Thus, we propose AhR as a target for *MYCN*-amplified neuroblastoma and that its antagonism, combined with current standard-of-care, may result in a more durable response in patients.

INTRODUCTION

Neuroblastoma is a malignancy arising from cells of the developing sympathetic nervous system and is the most common extracranial tumor in children.[1,2] Despite intensive, multi-modality treatments, approximately 50% of patients with high-risk neuroblastoma die of progressive or recurrent disease.[1–4] Moreover, long-term survivors develop a long list of side effects from the treatment, exacerbating the morbidity associated with high-risk neuroblastoma and underscoring the need for better therapeutic approaches.[4] While retinoic acid therapies have provided clinical benefit by inducing differentiation of neuroblastoma cells in patients with minimal residual disease, many patients eventually experience relapses due to insurgence of therapy resistance[3,5–7] and escaping the differentiation imparted by retinoids. The mechanisms that contribute to escape from retinoid-mediated differentiation are not fully understood.

MycN is a member of the Myc family of basic-helix-loop-helix zipper transcription factors, and its expression is mainly restricted to embryonic development.[8] MycN is a major transcriptional driver of neuroblastoma progression, and its amplification is present in 40–50% of high-risk patients. Amplification of *MYCN* is an unfavorable factor for survival and correlates with poor patient prognosis and poor response to retinoic acid treatment.[9–11]

The aryl hydrocarbon receptor (AhR) is a ligand-activated transcription factor that is kept inactive in the cytoplasm through interaction with chaperone proteins and upon ligand binding translocates to the nucleus to modulate gene expression.[12] While AhR was originally discovered for its role in mediating xenobiotic metabolism,[13,14] recent studies have demonstrated that AhR plays an important role in cancer biology. However, its exact functions in tumors are quite controversial, as previous studies have demonstrated that AhR can act as an oncogene in some settings[15–20] but as a tumor suppressor in others,[21–26] sometimes with conflicting or contradictory reports.[18,19,23,27–29] Additionally, AhR has been shown to promote, suppress, or have no effect on the expression of Myc family proteins depending on the cancer cell type and cellular context.[15,21,30] The role of AhR as a regulator of *MYCN*-amplified neuroblastoma progression remains incompletely characterized.

While no AhR antagonists are currently approved for cancer treatment, a few of them are either FDA-approved for different indications (i.e., clofazimine) or currently in clinical trials (i.e., BAY-2416964). Importantly, clofazimine has been safely used in children with leprosy, multi-drug resistant tuberculosis, and other infections with no adverse effects.[31,32]

[1]Department of Cell Stress Biology, Roswell Park Comprehensive Cancer Center, Buffalo, NY, USA
[2]Department of Pharmacology and Therapeutics, Roswell Park Comprehensive Cancer Center, Buffalo, NY, USA
[3]Department of Biochemistry and Neurology, Institute for Myelin and Glia Exploration, State University of New York at Buffalo, Buffalo, NY, USA
[4]Department of Medical Biotechnology and Translational Medicine, University of Milan, Foundation I.R.C.C.S. Carlo Besta Neurological Institute Milan, Italy
[5]Department of Biostatistics and Bioinformatics, Roswell Park Comprehensive Cancer Center, Buffalo, NY, USA
[6]Department of Pediatric Oncology, Roswell Park Comprehensive Cancer Center, Buffalo, NY, USA
[7]Lead contact
*Correspondence: Mark.Long@RoswellPark.org (M.D.L.), Anna.Bianchi-Smiraglia@RoswellPark.org (A.B.-S.)
https://doi.org/10.1016/j.isci.2023.108303
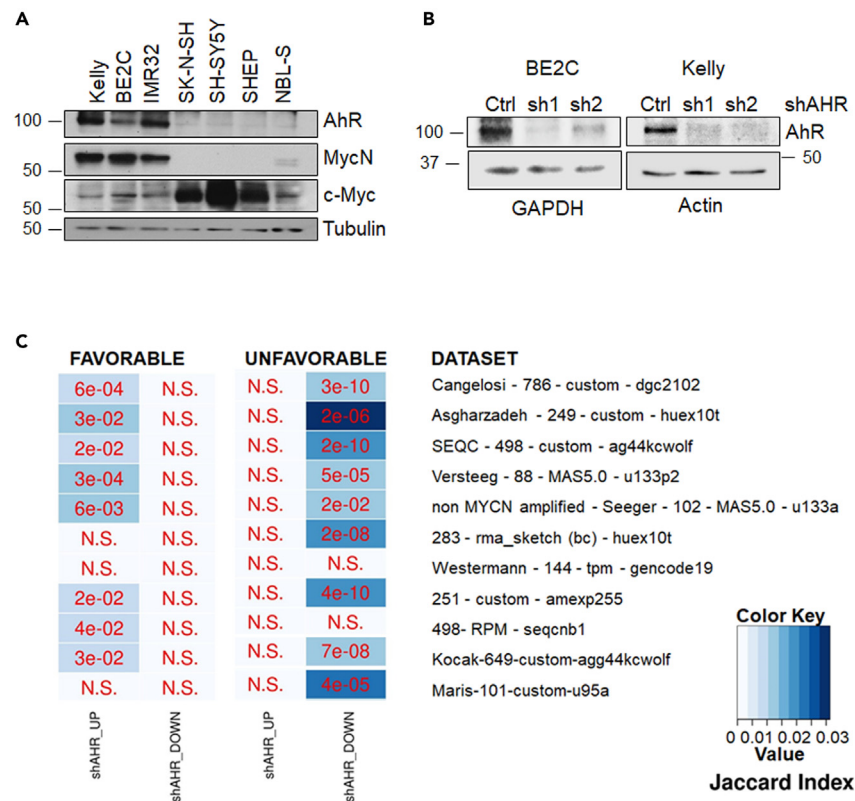
Figure 1. AhR associates with MycN and with poorer prognosis in neuroblastoma

(A) Immunoblot for AhR, MycN, and c-Myc in a panel of neuroblastoma cell lines with or without *MYCN* amplification. Tubulin is used as loading control.

(B) Immunoblot of BE2C and Kelly cells transduced with two independent shAHR constructs and their corresponding non-silencing control vector. Actin or GAPDH are used as loading control.

(C) Overlaps between genes from our shAHR_UP and shAHR_DOWN gene signatures and published favorable and unfavorable gene signatures derived from 11 neuroblastoma datasets. Statistics performed with hypergeometric test. Jaccardi index was used to compare the similarity. See also Figures S1 and S2, Tables S1 and S2.

Here, we report that AhR acts as a tumor promoter in the context of *MYCN*-amplified neuroblastoma, partly through MycN regulation but also via MycN-independent suppression of differentiation. Furthermore, we show that AhR pharmacological antagonism with clofazimine potentiates retinoic acid treatment efficacy *in vitro* and *in vivo*. Thus, our study identifies AhR as a potential therapeutic target in *MYCN*-amplified neuroblastoma.

RESULTS

AhR acts as a tumor promoter in *MYCN*-amplified neuroblastoma

Immunoblot analysis of a panel of human *MYCN*-amplified and non-amplified cell lines revealed a positive correlation in protein expression between AhR and MycN and an inverse correlation with cMyc (Figure 1A). MycN and cMyc are known to have opposite patterns of expression in neuroblastoma[33–35] and our data open the possibility that AhR may play different roles in *MYCN*-amplified versus non-amplified neuroblastoma. AhR expression levels may not necessarily represent levels of AhR activity.[36] To assess whether AhR transcriptional activity (which assesses AhR's functionality) has any correlation with neuroblastoma survival, we chose two human *MYCN*-amplified neuroblastoma cell lines (BE2C and Kelly) that showed detectable expression of AhR protein (Figure 1A) and depleted AHR with two lentiviral shRNA constructs that we previously validated[15] or their corresponding non-silencing control (Figure 1B). We then performed RNA-seq and extracted a signature of 123 genes that were commonly upregulated (shAHR_UP) and 135 genes that were commonly downregulated (shAHR_DOWN) by the two shAHR constructs in both cell lines, with an absolute fold change ≥1.5 and adj. p < 0.05 (Figure S1; Table S1). We overlapped the "shAHR_UP" and "shAHR_DOWN" gene lists with recently reported "favorable" and "unfavorable" survival gene signatures from 11 neuroblastoma patients' datasets[37] that are hosted on the R2 database. These datasets contain both *MYCN*-amplified and non-amplified patients, with the non-amplified representing most of the cases. The shAHR_UP genes significantly overlapped with genes found in the favorable signatures, while the shAHR_DOWN genes significantly overlapped with genes in the unfavorable signatures (Figure 1C). At the same time, interrogation of two widely used datasets, SEQC and "Therapeutically Applicable Research to Generate Effective Targets project" (TARGET),
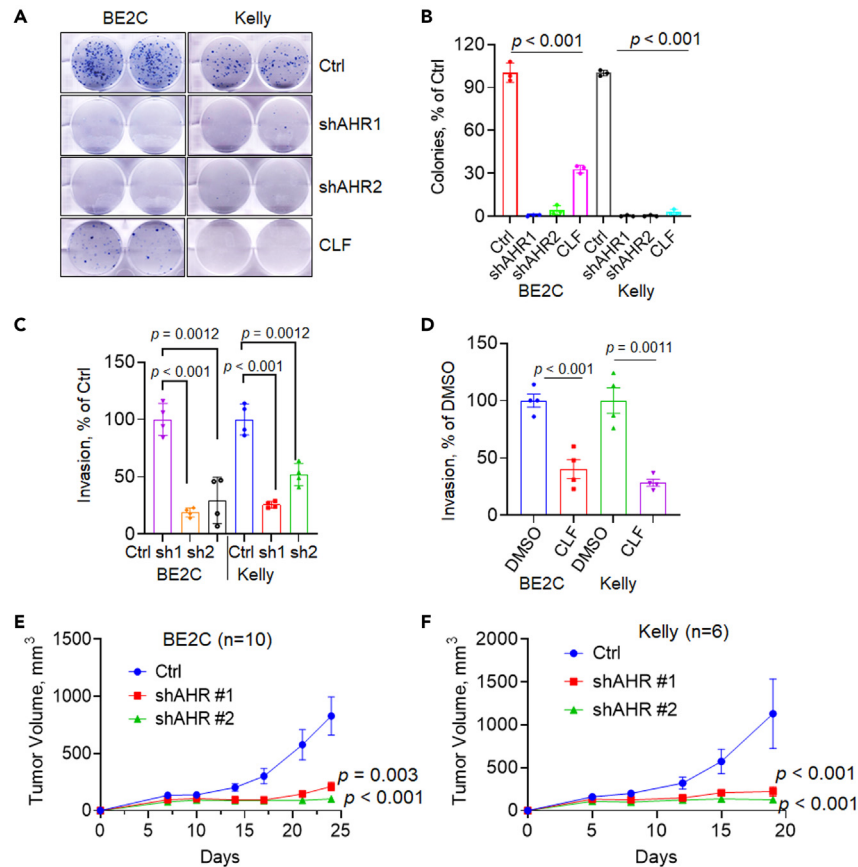
Figure 2. AhR is a tumor promoter in *MYCN*-amplified neuroblastoma

(A) Representative clonogenic assay (out of 3) of BE2C and Kelly cells transduced with two independent shAHR constructs and their corresponding non-silencing control vector or treated with the AhR antagonist clofazimine (CLF, 2 μM Kelly, 4 μM BE2C).

(B) Quantification of (A) performed with ImageJ. Statistics by two-tailed Student's *t* test. Data are average −/+ SD (n = 3).

(C) Invasion assay of *MYCN*-amplified human neuroblastoma BE2C and Kelly cells transduced with two independent shAHR constructs and their corresponding non-silencing control vector. Data are average −/+ SD (n = 4). Statistics by two-tailed Student's *t* test.

(D) Invasion assay of BE2C and Kelly cells treated for a total of 48hrs with CLF (4 μM BE2C, 2 μM Kelly). Data are average −/+ SD (n = 4). Statistics by two-tailed Student's *t* test.

(E) BE2C or (F) Kelly cells transduced as in (D) were injected SQ in the right flank of NSG mice (n = 10 for BE2C and n = 6 for Kelly). Equal numbers of females and males were used. Tumors were measured twice/week. Animals were humanely euthanized when a tumor in any group reached the limits set by IACUC protocol. Data are average −/+ SEM. Statistics by two-way ANOVA test. See also Figure S3.

revealed inconsistent association between AHR mRNA levels (split on median) and the overall survival of patients (Figures S2A–S2F). In the SEQC dataset a positive correlation between AHR levels and survival was detected when analyzing the entirety of the set, similarly to what was previously reported,[26] as well as in the non-*MYCN*-amplified subset (Figures S2C and S2E), but no difference in survival was observed with *MYCN*-amplified patients (Figure S2A). Interestingly, analysis of the TARGET dataset did not reveal any association independently of the stratification (Figures S2B, S2D, and S2F). Together, these data suggest that AhR transcriptional activity is detrimental to the survival of neuroblastoma patients and could potentially have better prognostic value than AHR mRNA levels.

We assessed the consequences of AHR depletion in *MYCN*-amplified neuroblastoma cells and found that the clonogenic potential of BE2C and Kelly cells depleted of AHR, either genetically or pharmacologically with the AhR antagonist clofazimine (CLF)[15] (Figures 2A and 2B), as well as their invasive capability (Figures 2C and 2D) were reduced compared to control cells. Pharmacological inhibition of AhR with three additional antagonists, including the classical AhR antagonist CH-223191,[38] BAY-2416964 (clinical trials NCT04069026 and NCT04999202), and KYN-101[39] yielded similar results (Figure S3A).

Conversely, AHR ectopic expression in the same cells led to a ∼2-fold increase in invasion (Figure S3B), supporting a pro-tumorigenic function of AhR in *MYCN*-amplified neuroblastoma cells. Interestingly, previous reports have suggested that AhR acts as a tumor suppressor in neuroblastoma cells, especially those of non-*MYCN*-amplified origin.[25] AHR ectopic expression in human non-*MYCN*-amplified SK-N-SH and SH-SY5Y cells resulted in a reduction in clonogenic growth (Figure S3C) and a slight reduction in invasion capability (Figure S3D), corroborating previous findings,[25,26] as well as in a reduction in cMYC protein levels (Figure S3E) while MycN was virtually undetectable. Thus, AhR
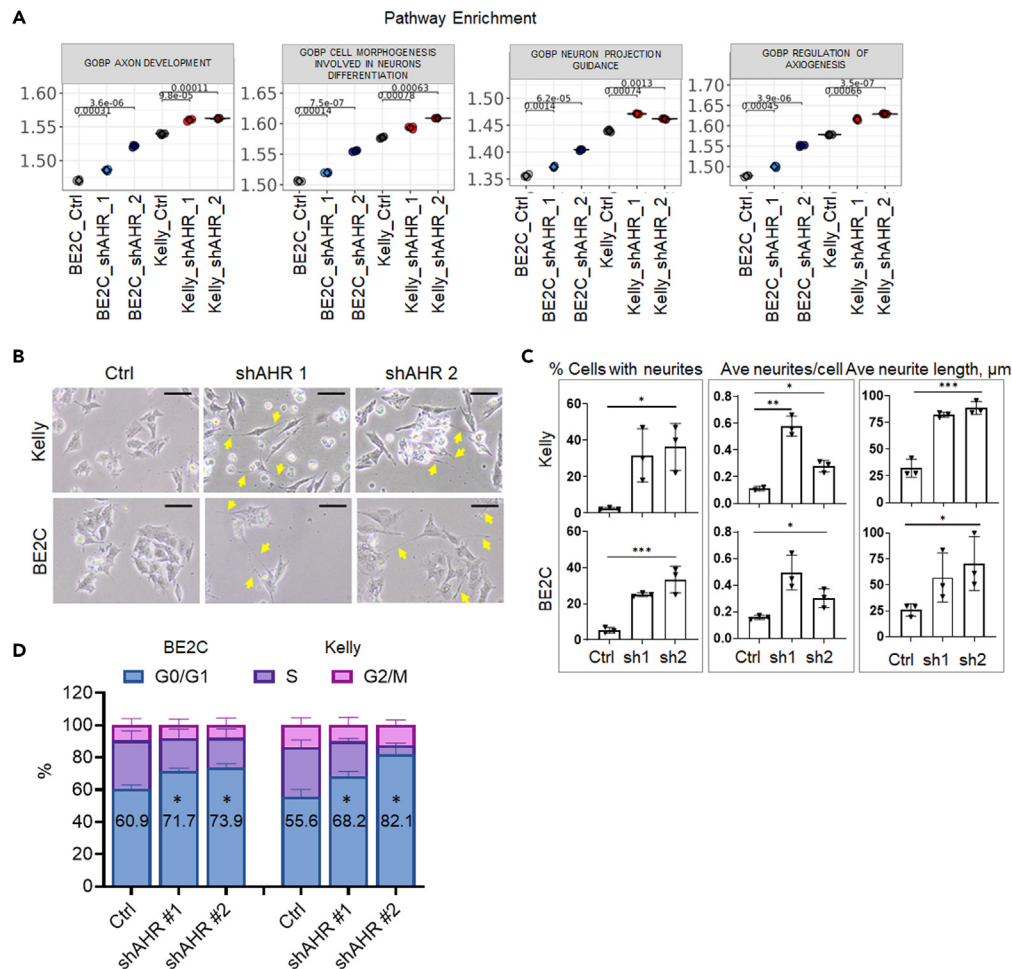
Figure 3. AhR suppresses differentiation

(A) GSVA pathway enrichment analysis for several neuronal-related pathways from RNA-seq of BE2C and Kelly cells transduced with two independent shAHR constructs and their corresponding non-silencing control vector.

(B) Representative phase contrast images of cells as in (A). Scale bar is 100 μm. Arrows point to neurites.

(C) Quantification of % cells with neurites, average neurites/cell, and average neurite length from 3 independent experiments as in (A). Data are average −/+ SD. Statistics by two-tailed Student's *t* test *p < 0.05; **p < 0.001; ***p < 0.0001.

(D) Cell cycle analysis of cells as in (A). Data are average −/+ SD of 3 independent experiments. Statistics by two-tailed Student's *t* test. *p < 0.05. See also Figures S4 and S5.

appears to have a previously unrecognized dual role in neuroblastoma, as a tumor promoter or tumor suppressor depending on the *MYCN*-amplification status.

Finally, BE2C and Kelly cells depleted of AHR failed to grow tumors *in vivo* when implanted subcutaneously (SQ) into the flank of immunocompromised NOD SCID-gamma (NSG) mice (Figures 2E and 2F).

Altogether, these data strongly suggest that AhR acts as a tumor promoter in *MYCN*-amplified neuroblastoma.

AhR suppresses differentiation of *MYCN*-amplified neuroblastoma cells

Gene Ontology (GO) analysis of the aforementioned RNA-seq showed a significant upregulation of neuronal differentiation signatures in both BE2C and Kelly cells upon AHR depletion (including genes such as STMN4[40] and EFNA2,[41] Table S1), with concomitant suppression of processes associated with cell cycle progression (Figures 3A and S4A; Table S2). These findings were further confirmed at a morphological level, with AHR depletion causing cellular morphological changes, consistent with induction of neuronal differentiation, such as the appearance of cell neurite projections (Figures 3B and 3C). Immunostaining for *bona fide* neurite markers tubulin beta 3 (Tubb3)[42,43] and neurofilament (Nefl)[44] confirmed the nature of the neurites (Figures S4B and S4C). Similar morphological changes were observed upon AhR pharmacological inhibition with CLF, CH-223191, BAY-2416964, and KYN-101 in BE2C cells (Figure S4D). Finally, AHR-depleted cells were found to accumulate in G_0/G_1 phase (Figure 3D) which is conducive to differentiation.[45]

Inhibition of MycN in *MYCN*-amplified cells is also known to induce differentiation.[46] AHR depletion by shRNA in both cell lines resulted in reduced MYCN RNA (Figure S5A) and protein (Figure S5B) levels, while AhR activation with its prototypical ligand TCDD did not cause any significant changes in MycN levels (FigureS5C). Consistently, AHR depletion resulted in down-regulation of Myc-related signaling, as evidenced by GSVA and gene set enrichment analysis (GSEA) pathway enrichment analysis of differentially expressed genes (Figures S5D and S5E), as well as down-regulation of established MYCN target genes such as MDM2[47] and PTMA[48] (Figure S5F). Similarly, AhR pharmacological inhibition with the four antagonists described previously caused a reduction in MycN levels (Figure S5G). To investigate whether AhR's effects on differentiation are linked to its ability to regulate MycN, we depleted BE2C and Kelly cells of MYCN via siRNA, with or without concomitant ectopic expression of AHR (Figure S5H). While MYCN depletion induced morphological changes and neurites outgrowth, as previously reported,[46] AHR over-expression was able to inhibit this process (Figures S5I and S5J).

These data suggest a unique role for AhR in the regulation of neuroblastoma differentiation.

AhR is involved in chromatin remodeling

It is well-established that cellular differentiation is characterized by changes in chromatin accessibility.[49] To further examine how AhR regulates the differentiation of *MYCN*-amplified neuroblastoma cells, we performed Assay for Transposase-Accessible Chromatin (ATAC)-sequencing in BE2C and Kelly cells with or without AHR depletion. Although most ATAC-seq peaks were found to be promoter proximal, as expected with this method (Figure 4A, *top six rows*), when we assessed the relative distribution of the "gained" and "lost" open regions in AHR-depleted cells, we found that most of the differentially accessible regions (DARs) were residing distal (10–100 Kb) to transcription start sites (TSSs) (Figure 4A, *bottom four rows*).

In order to gain insight into what types of genomic regions exhibited altered open chromatin in response to knockdown of AHR, we performed ChromHMM[50] using publicly available ChIP-seq data from Kelly cells (GSE138314)[51] using the histone marks H3K4me1 (enhancer region), H3K4me3 (promoter region), H3K27me3 (repressive state), and H3K27ac (active state) to characterize the DARs from our own Kelly ATAC-seq. The analysis revealed that both gained and lost DARs were highly enriched for active enhancers (Figure 4B), with active enhancers making up only ~10% of total genomic space in Kelly cells but making up ~45% and 75% of genomic space among the gained and lost DARs, respectively. These data suggest a strong enhancer reprogramming effect upon AHR knockdown. Given that super-enhancers (SEs) are known to drive transcription factors governing cell identity,[52,53] we first went back to ChIP-seq data from Kelly cells (GSE138314)[51] and defined active super enhancers (SE) using the active histone mark H3K27ac with the ROSE (Rank Ordering of Super Enhancers) algorithm.[54] We next compared regions that lost accessibility upon AHR knock-down (lost DARs) with active SEs identified in Kelly cells and found a significant overlap (Figure 4C). Motif analysis revealed that 18/21 of these overlapping regions contained binding sites for AP-2 (a master regulator of the mesenchymal phenotype in neuroblastoma) and that 7 of the 11 transcription factor motifs found drive mesenchymal transcriptional programs in neuroblastoma[55] (Figure 4D, red bars).

To gain a broader view of the transcription factors whose access to chromatin may be altered upon AHR knockdown, we used the GIGGLE genomic inquiry tool to overlap all of the DARs identified by ATAC-seq with CistromeDB and found that lost DARs were enriched in known binding regions for Myc and MycN (and their binding partner MAX) as well as with those for AP-2, in agreement with the aforementioned analysis (Figures 4E and 4F). On the other hand, gained DARs aligned strongly with binding regions for PHOX2B, GATA2/3, and RARA (Figures 4E and 4F) which are known drivers of neuronal differentiation.[56,57]

Together, these findings indicate that knockdown of AHR alters chromatin accessibility at regions distal to transcriptional start sites and enriches for predicted enhancers and SEs. Moreover, regions that lose accessibility strongly enrich for binding of transcription factors of the MYC and AP-2 family known to promote a mesenchymal phenotype, while regions that gain accessibility enrich for RARA and other drivers of neuronal differentiation. These observations at the genomic level are consistent with the phenotypic and morphological changes observed in Figure 2 upon knockdown or antagonism of AhR, as well as the global gene expression changes observed.

These findings suggest that antagonism or loss of AhR leads to enhancer reprogramming, thus affecting the differentiation potential of *MYCN*-amplified neuroblastoma cells.

AhR inhibition synergizes with retinoic acid therapy in *MYCN*-amplified neuroblastoma

The aforementioned ATAC-seq findings raised the possibility that AHR depletion could affect the response to retinoic acid-based therapy. This was further supported by detection of induction of established all-trans retinoic acid (ATRA) target genes upon AHR depletion in our RNAseq, such as SCG2,[58] NAV2,[59] CREB5,[60] NBL1,[60] and FZD7[60] (Figure 5A). To investigate this, BE2C and Kelly cells depleted or not of AHR were treated with ATRA and we found that AHR depletion augmented retinoic acid-induced differentiation, as measured by percent of cells with neurites, average number of neurites per cell, and average neurite length relative to treatment with retinoic acid alone (Figures S6A–S6D). Moreover, AHR depletion potentiated the ATRA-induced suppression of MycN (Figures S6E and S6F).

Consistently, CLF-mediated AhR antagonism and ATRA treatment induced stronger morphological changes in cells when combined than singularly (Figure 5B), as well as almost completely abolished colony formation at doses at which the single drugs were not as effective (Figures 5C and 5D). Similar to the genetic depletion, the combination of CLF and ATRA resulted in a stronger suppression of MycN levels than control or treatment with either drug alone (Figure 5E).

To test for potential synergy between CLF and ATRA, BE2C and Kelly cells were treated with several combinations of the drugs, centered around their IC_{50} and the proportions of surviving cells were analyzed with CompuSyn. The analysis revealed a strong synergistic effect of CLF and ATRA in suppressing the growth of BE2C and Kelly cells, as indicated by a combination index (CI) of less than 1 (Figure 5F).
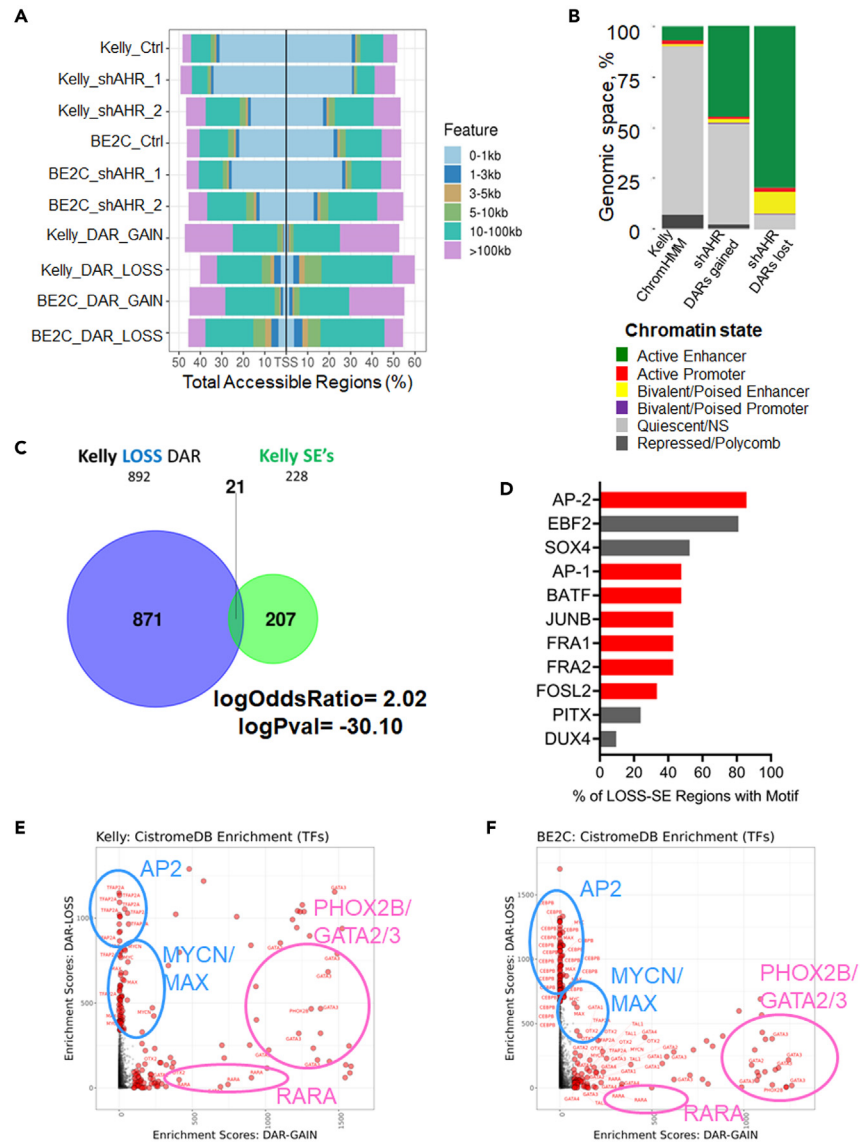
Figure 4. AhR is involved in chromatin remodeling at distal regions

(A) Peaks of accessible chromatin across 3 replicates/sample (top 6 rows) and differentially accessible regions (DARs, bottom 4 rows) identified by ATAC-seq in Kelly and BE2C cells transduced with control vector or depleted of AHR.

(B) ChromHMM analysis based on ChIP-seq data in Kelly cells identifies active enhancers as highly enriched in DARs upon AhR knockdown.

(C) Significant overlap between lost DARs and super-enhancers (SEs) defined in Kelly cells.

(D) Significant motifs identified in 21 lost DARs that overlap with SEs. Red bars indicate TFs associated with less differentiated phenotype. GIGGLE analysis to compare DARs with known binding sites for over 9,000 transcription factors in Kelly (E) or BE2C (F) cells.

To assess the degree of persistence of differentiation upon drug treatment, cells were treated with CLF, ATRA, their combination, or DMSO as vehicle control for 10 days to induce differentiation. At that point (day 0 in Figure S7), cells were released from the drugs and cultured in complete media alone for up to 25 days. Control cells continued to grow regularly and needed to be split every 2–3 days; clofazimine-treated cells resumed growth and de-differentiated morphology within a couple of days and, similar to control, needed to be split every 2–3 days. ATRA-treated cells took about a week to restart growing with normal doubling time and morphology. The CLF+ATRA cells maintained the differentiated morphology throughout the 25 days and did not resume growth (Figure S7). These data suggest that the combination of CLF and ATRA is more efficient in inducing a stable differentiation of cells.

To test whether the combination would also be more effective in an *in vivo* setting, we pretreated cells with either drug alone, their combination, or vehicle control, to mimic minimal residual disease settings as previously reported.[61] Equal numbers of live cells were implanted SQ in NSG mice, with no further treatment. While vehicle control cells and single drug-treated cells formed rapidly
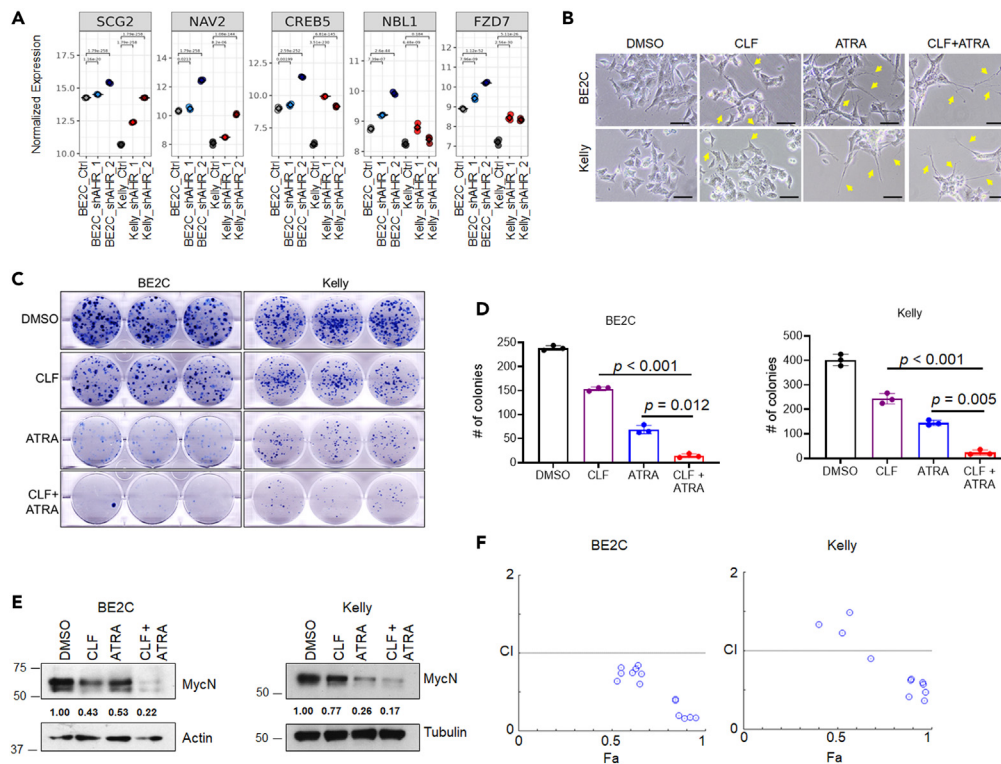
Figure 5. Clofazimine and ATRA are synergistic *in vitro*

(A) Normalized expression of selected ATRA-induced genes from the RNAseq analysis.

(B) Representative phase contrast images of BE2C and Kelly cells treated with 4 μM CLF, 10 μM ATRA, or a combination of the two for 7 days. Scale bar is 100 μm.

(C) Representative clonogenic assay (out of 3) of BE2C and Kelly cells treated with 1 μM CLF, 2 μM (Kelly) or 5 μM (BE2C) ATRA, or a combination of the two.

(D) Quantification of (C) performed with ImageJ. Statistics by two-tailed Student's *t* test. Data are average −/+ SD (n = 3).

(E) Representative immunoblot for MycN in BE2C and Kelly cells treated as in (A). Actin or tubulin are used as loading control. Quantifications performed with ImageJ: MycN signal was normalized to that of the corresponding loading control and then normalized to the value of DMSO.

(F) CompuSyn-based analysis of synergy between CLF and ATRA in BE2C and Kelly cells. Cells were treated with several combinations of the drugs, centered around their IC_{50} (CLF 0-6 μM; ATRA 0-80 μM) for 48 hrs. Surviving cells were stained with methylene blue. Most of the combinations have a CI below 1 indicating synergy. See also Figure S6.

growing tumors, the combination strongly suppressed tumor growth (Figures 6A and 6B). Statistical analysis comparing the combination group to control or either single drug showed a statistically significant (p = 0.001) difference, indicating a synergistic effect (Figure 6A). Tumors sections were stained for Tubb3 and MycN. CLF and ATRA as single agents showed an increase in staining intensity for the differentiation marker Tubb3 (Figure 6C) and a reduction in MycN (Figure 6D). Their combination was significantly more potent at inducing this differentiation phenotype, in agreement with the almost negligible growth of the xenografts in mice (Figures 6A and 6B).

Overall, our study unveils a previously undisclosed pro-tumorigenic function of AhR in *MYCN*-amplified neuroblastoma, centered on its ability to suppress differentiation. These functions pass partly through regulation of chromatin accessibility, which negates retinoic acid-induced signaling and supports MycN functions. Most importantly, our data highlight AhR as a potential target in the treatment of *MYCN*-amplified neuroblastoma, whereby AhR antagonism may prime the cells to be responsive to retinoic acid treatment and synergize with retinoid-based therapy. As a few AhR antagonists are already in clinical trials and/or FDA-approved for other interventions, our data provide the basis for their repurposing into future pre-clinical and clinical trials for *MYCN*-amplified neuroblastoma.

DISCUSSION

The tumorigenic role of AhR in the nervous system and particularly in neuroblastoma is only beginning to emerge and remains largely understudied and controversial, with different groups reporting different effects of AhR activation or inhibition on neuroblastoma cell fate.[25,26,62–66] Our findings revealed that in *MYCN*-amplified neuroblastoma, AhR acts as a tumor promoter, supporting tumor growth, positively regulating MycN levels, and maintaining cells in an undifferentiated state. Similarly, AhR activation by low doses of its prototypical ligand TCDD has been shown to enhance neuroblastoma cell migration[66] and parental exposure to various AhR ligands has been loosely linked to higher odds of neuroblastoma development in their offspring.[67]
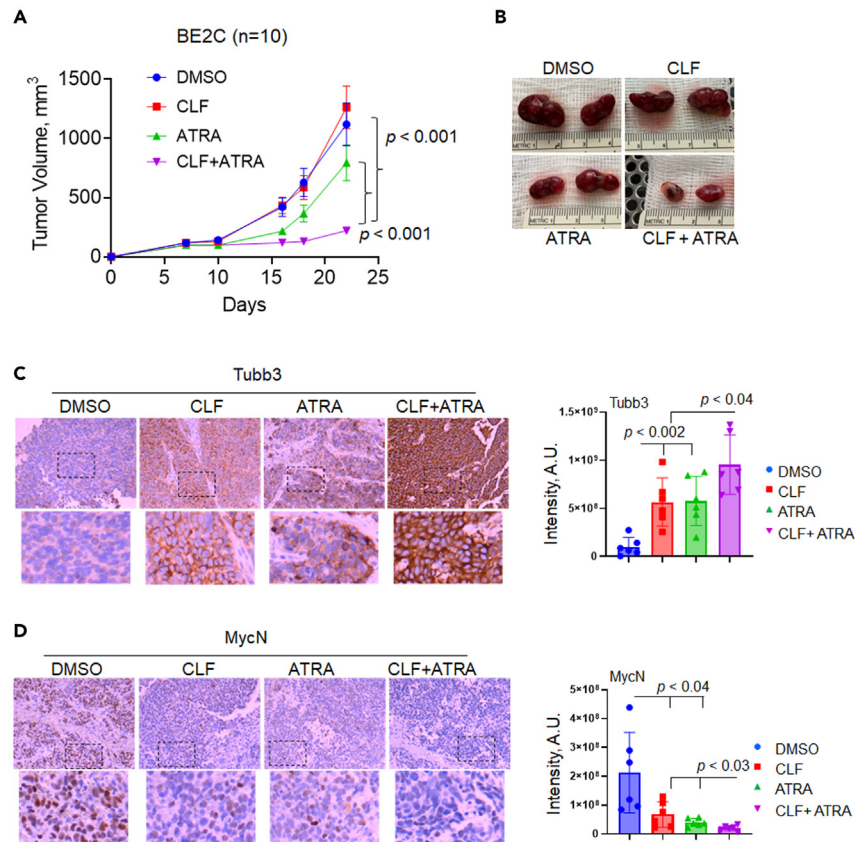
Figure 6. Clofazimine and ATRA are synergistic *in vivo*

(A) BE2C cells treated with 6 μM CLF, 10 μM ATRA, or a combination of the two for 7 days were injected SQ in the right flank of NSG mice (n = 10, equal numbers of females and males were used). Tumors were measured with a caliper twice/week. Animals were humanely euthanized when a tumor in any group reached the limit set by IACUC protocol. Data are average −/+ SEM. Statistics by two-way ANOVA test. Representative tumor pictures are shown.

(B) Representative images of tumors excised at the endpoint of (A).

(C and D) Representative IHC images and quantification of tumor sections from (A) stained for Tubb3 (C) and MycN (D). Data are average −/+ SD (n = 6). Statistics by two-tailed Student's *t* test. See also Figure S7.

On the other hand, AHR ectopic expression has been suggested to induce differentiation in mouse Neuro2a cells, which do not otherwise express endogenous AhR[63] and miR-124-mediated suppression of AhR has been linked to suppression of differentiation in SK-N-SH cells.[64] However, miR-124 is actively up-regulated during induction of differentiation in SH-SY5Y cells[68] (which are a derivative of SK-N-SH) thus adding to the controversy. Wu et al.[25] reported AhR to be a tumor suppressor in neuroblastoma through MycN downregulation: these studies mostly interrogated AhR function and regulation of MycN expression in non-*MYCN*-amplified neuroblastoma, where MycN is not a driver of the disease and in cells that, according to our results and published ones[26,69] do not have detectable levels of endogenous AhR protein.

In our hands, AHR overexpression in these cell systems leads to downregulation of cMyc, which is highly expressed in non-*MYCN*-amplified cells and contributes to their tumorigenicity. Consistently, upon AHR depletion we observed a reduction in clonogenic growth and invasion of non-*MYCN*-amplified cells, while we could not detect MycN protein levels. In order to observe neurite outgrowth, Wu et al.[25] kept AHR-overexpressing cells in constant selective antibiotic for a month, which may have led to unintended consequences in terms of cell stress or mutations and may explain some of the discrepancies with our data. In our current work, only 48-72 hrs of antibiotic selection after lentiviral delivery of shAHR were applied and neurite outgrowth, whose nature was confirmed by immunofluorescence for neurite markers, was observed within a week.

Altogether, these results highlight a previously unrecognized opposing role of AhR in different neuroblastoma subtypes, similar to what has been reported in different breast cancer subtypes.[18,19,70,71] The data obtained in non-*MYCN*-amplified cells suggest that AhR's anti-tumor functions in these settings are independent of MycN and may depend instead on other nuclear factors and receptors being expressed differently between the subtypes, such as cMYC. This hypothesis is also consistent with the notion that AhR can act very differently during organismal development and during tumor progression. For instance, a recent paper reported novel endogenous ligands of AhR that mediate neural development in zebrafish[72] and previous work suggested that crossing AHR knock-out mice with the TRAMP model results in promotion of prostate carcinogenesis[73] as well as colon carcinogenesis in the Apc/Kras mice background.[74] However, AhR manipulation in cancer cells

from both prostate and colon cancer suggest a tumor promoting role of AhR.[65,75] Thus, the role of the nuclear milieu in terms of factors and co-factors potentially influencing AhR activity needs to be explored in depth and may help better understand the shift in functions of AhR and shed light on some of the controversies surrounding AhR biology.

AhR is normally sequestered in an inactive form in the cytoplasm and becomes active once it is released and allowed to translocate to the nucleus where it activates gene transcription. Thus, AhR levels per se (at RNA or protein level) are not necessarily indicative of its activity. Wu et al. reported that AHR mRNA levels (stratified by average level of expression) associated with differences in patients' survival when interrogating the SEQC dataset[26]; however, this relationship does not exist when restricting the analysis to MYCN-amplified patients in this same dataset nor in the "Therapeutically Applicable Research to Generate Effective Targets project" (TARGET) independently of patients' stratification. Since the anti-tumor effects of AhR were proposed to be through its ability to suppress MYCN[25,26] but MycN is not a driver in non-MYCN-amplified neuroblastoma, the significance of this association needs to be reevaluated as what these data altogether suggest is that AhR tumor suppressive roles in non-MYCN-amplified neuroblastoma might be through other factors (such as possibly cMYC). Similarly, the survival analyses between AhR protein expression and different types of neuroblastoma (undifferentiated, differentiating, and ganglioneuroblastoma)[26] will need to be re-evaluated separating cohorts on median or average expression of AhR rather than scanning for the best separation groups, as well as analyzing the correlation with nuclear localized (active) AhR rather than total. Several AhR transcriptional activity gene signatures have been described[17,36]; however, they were mainly derived from studies in epithelial cells. In order to obtain neuroblastoma-relevant genes, we created a signature from genes that were consistently regulated upon AHR depletion with two independent shRNA constructs in two MYCN-amplified human neuroblastoma cell lines, thus enhancing the stringency of the analysis. Interestingly, this gene signature strongly aligns with a favorable outcome in several distinct patients' datasets,[37] which yet contain >70% non-MYCN-amplified cases. Thus, it will be important in the future to carefully evaluate the effects of AhR antagonism on patient-derived organoids or xenografts to assess any confounding effect due to tumor heterogeneity.

ATAC-seq experiments revealed that AhR can affect chromatin accessibility at distal regions, in agreement with previous reports of AhR's ability to promote DNA hypermethylation[76,77] and to participate in epigenetic regulatory complexes.[78,79] Neuroblastoma has been shown to be composed of interchangeable populations of mesenchymal and adrenergic subtypes.[53,55] The mesenchymal subtype is considered to be more undifferentiated and therapy-resistant and is enriched post-treatment and in relapsing tumors.[53,55] The adrenergic subtype is more committed and therapy-responsive.[53,55] The transcription factors PHOX2B, GATA2/3, and HAND1/2 are associated with the SE circuitry that defines the adrenergic lineage and control neuronal specification and differentiation during development.[55,80,81] The levels of these transcription factors need to be tightly regulated in cells as high levels are deleterious and correlate with poor survival.[82–84] Consistently Zimmerman et al.[85] reported GATA3 and PHOX2B to be downregulated during ATRA-induced differentiation. Thus, dosage of these transcription factors appears to be critical where low levels may promote differentiation while too high levels drive neuroblastoma progression. In our RNA-seq data, we see a trend toward small but significant downregulation of PHOX2B and GATA3 upon AHR-downregulation, although this is not fully consistent among constructs. At the same time, we see opening of chromatin loci bound by these factors when cells are depleted of AHR. Thus, it is possible that reduced levels of PHOX2B and GATA3 binding at newly opened regions may help drive differentiation, consistent with their biological role during differentiation.

Notably, we found that AHR depletion induced opening at regions commonly bound by RARα and restricted access to regions commonly bound by MycN. These data imply that AHR depletion would suppress MycN related signaling and potentially prime the cells for retinoic acid-mediated signaling and induction of differentiation. Indeed, RNA-seq analysis yielded results consistent with this hypothesis, which was further validated morphologically and by immunostaining. Interestingly, AHR ectopic expression was able to counteract the differentiation caused by MYCN depletion, suggesting that AhR may work independently of (or perhaps in parallel with) MycN in regard to differentiation. These findings add to the growing complexity and controversy on the topic of the AhR-Myc family interaction and cross-regulation.[21,25,26,30,86–89]

Treatment of patients with high-risk MYCN-amplified neuroblastoma remains a clinical challenge, as relapses resulting from the residual tumor cells' ability to overcome differentiating therapies such as retinoic acid occur in more than 50% of patients.[90] We find that the retinoic acid effects are potentiated when AhR is inhibited either genetically or pharmacologically, suggesting a potential synergy between AhR inhibition and retinoid treatment to achieve a more durable response. Consistently, injection of cells pre-treated with the combination of CLF and ATRA, in order to mimic minimal residual disease settings occurring in patients, prevented the growth of tumor xenograft in mice suggesting that the differentiation imparted by both drugs is more durable and less easy to overcome than the one imparted by the individual drugs. The AhR antagonist CLF is already FDA-approved for the treatment of leprosy, drug-resistant tuberculosis, and other infections and has been safely used in children with no adverse effects[31,32,91,92] and our studies showed that CLF synergistically enhances the effectiveness of retinoic acid in MYCN-amplified neuroblastoma. Of the two novel AhR antagonists used in this study, BAY-2416964 is currently in Phase I clinical trials for advanced solid tumors (NCT04069026 and NCT04999202) and KYN-101 demonstrated anti-tumor efficacy in pre-clinical murine models of melanoma.[93] Importantly, the differentiation imparted by the combination of CLF and ATRA on cultured cells was sustained for up to 25 days post-drug withdrawal, while the single drug treated cells resumed growth within a week, consistent with the in vivo data. Thus, it will be important to thoroughly evaluate the synergy between treatment with AhR antagonists and retinoids in multiple pre-clinical models of the disease as a means to ensure a more durable response in patients.

Limitations of the study

Our study showed that pre-treatment of cells with clofazimine and retinoic acid to mimic induction of minimal residual diseases reduce their growth in vivo and maintain the cells in a differentiated-like status for longer. However, it will be important to use a

better model of minimal residual disease mimicry, such as implanting naive cells, letting tumors grow, treat them with conventional therapy until regressed, and then administer the drug combination. Similarly, it will be important to test the drug combination in a relevant model of the disease, such as the TH-*MYCN* mice, where the effects from and upon the immune system are also kept in consideration.

STAR★METHODS

Detailed methods are provided in the online version of this paper and include the following:

- KEY RESOURCES TABLE
- RESOURCE AVAILABILITY
  - Lead contact
  - Materials availability
  - Data and code availability
- EXPERIMENTAL MODEL AND STUDY PARTICIPANT DETAILS
  - Mouse models
  - Cell lines
- METHOD DETAILS
  - Lentiviral infections
  - Cell cycle analysis
  - Immunofluorescence
  - RNA-seq
  - ATAC-seq
  - ChromHMM
  - Super-enhancers identification
  - Motif analysis
  - Quantitative real-time PCR
  - Colony formation assays
  - Invasion assays
  - Immunoblotting
  - Neurite analysis
  - Immunohistochemistry staining
- QUANTIFICATION AND STATISTICAL ANALYSIS

SUPPLEMENTAL INFORMATION

Supplemental information can be found online at https://doi.org/10.1016/j.isci.2023.108303.

AUTHOR CONTRIBUTIONS

A.B-S., M.D.L., and K.A.C. designed the study; K.A.C., J.J.J., J.C.M., T.d.S.F., and E.H. performed experiments and analyzed data; B.M.G. performed the mouse studies; E.K. performed immunohistochemistry analysis; K.M.A. performed biostatistics analysis; M.L.F., C.J.T., D.J.S., M.D.L, and A. B-S. supervised the study and analyzed data. The manuscript was written by A.B.-S. and K.A.C. All authors discussed the results and commented on the manuscript.

DECLARATION OF INTERESTS

The authors declare no competing interests.

REFERENCES

1. Maris, J.M., Hogarty, M.D., Bagatell, R., and Cohn, S.L. (2007). Neuroblastoma. Lancet *369*, 2106–2120. https://doi.org/10.1016/S0140-6736(07)60983-0.

2. Matthay, K.K., Maris, J.M., Schleiermacher, G., Nakagawara, A., Mackall, C.L., Diller, L., and Weiss, W.A. (2016). Neuroblastoma. Nat. Rev. Dis. Primers *2*, 16078. https://doi.org/10.1038/nrdp.2016.78.

3. Matthay, K.K., Villablanca, J.G., Seeger, R.C., Stram, D.O., Harris, R.E., Ramsay, N.K., Swift, P., Shimada, H., Black, C.T., Brodeur, G.M., et al. (1999). Treatment of high-risk neuroblastoma with intensive chemotherapy, radiotherapy, autologous bone marrow transplantation, and 13-cis-retinoic acid. Children's Cancer Group. N. Engl. J. Med. *341*, 1165–1173. https://doi.org/10.1056/NEJM199910143411601.

4. Cheung, N.K.V., and Dyer, M.A. (2013). Neuroblastoma: developmental biology, cancer genomics and immunotherapy. Nat. Rev. Cancer *13*, 397–411. https://doi.org/10.1038/nrc3526.

5. Garaventa, A., Poetschger, U., Valteau-Couanet, D., Luksch, R., Castel, V., Elliott, M., Ash, S., Chan, G.C.F., Laureys, G., Beck-Popovic, M., et al. (2021). Randomized Trial of Two Induction Therapy Regimens for High-Risk Neuroblastoma: HR-NBL1.5 International Society of Pediatric Oncology European Neuroblastoma Group Study. J. Clin. Oncol. *39*, 2552–2563. https://doi.org/10.1200/JCO.20.03144.

6. Shusterman, S., Naranjo, A., Van Ryn, C., Hank, J.A., Parisi, M.T., Shulkin, B.L., Servaes, S., London, W.B., Shimada, H., Gan, J., et al. (2019). Antitumor Activity and Tolerability of hu14.18-IL2 with GMCSF and Isotretinoin in Recurrent or Refractory Neuroblastoma: A Children's Oncology Group Phase II Study. Clin. Cancer Res. *25*, 6044–6051. https://doi.org/10.1158/1078-0432.CCR-19-0798.

7. Finklestein, J.Z., Krailo, M.D., Lenarsky, C., Ladisch, S., Blair, G.K., Reynolds, C.P., Sitarz, A.L., and Hammond, G.D. (1992). 13-cis-retinoic acid (NSC 122758) in the treatment of children with metastatic neuroblastoma unresponsive to conventional chemotherapy: report from the Childrens Cancer Study Group. Med. Pediatr. Oncol. *20*, 307–311. https://doi.org/10.1002/mpo.2950200407.

8. Pession, A., and Tonelli, R. (2005). The MYCN oncogene as a specific and selective drug target for peripheral and central nervous system tumors. Curr. Cancer Drug Targets *5*, 273–283. https://doi.org/10.2174/1568009054064606.

9. Cohn, S.L., and Tweddle, D.A. (2004). MYCN amplification remains prognostically strong 20 years after its "clinical debut. Eur. J. Cancer *40*, 2639–2642. https://doi.org/10.1016/j.ejca.2004.07.025.

10. Reynolds, C.P., Wang, Y., Melton, L.J., Einhorn, P.A., Slamon, D.J., and Maurer, B.J. (2000). Retinoic-acid-resistant neuroblastoma cell lines show altered MYC regulation and high sensitivity to fenretinide. Med. Pediatr. Oncol. *35*, 597–602. https://doi.org/10.1002/1096-911x(20001201)35:6<597::aid-mpo23>3.0.co;2-b.

11. Nguyen, T., Hocker, J.E., Thomas, W., Smith, S.A., Norris, M.D., Haber, M., Cheung, B., and Marshall, G.M. (2003). Combined RAR alpha- and RXR-specific ligands overcome N-myc-associated retinoid resistance in neuroblastoma cells. Biochem. Biophys. Res. Commun. *302*, 462–468. https://doi.org/10.1016/s0006-291x(03)00177-3.

12. Barouki, R., Coumoul, X., and Fernandez-Salguero, P.M. (2007). The aryl hydrocarbon receptor, more than a xenobiotic-interacting protein. FEBS Lett. *581*, 3608–3615. https://doi.org/10.1016/j.febslet.2007.03.046.

13. Denison, M.S., and Nagy, S.R. (2003). Activation of the aryl hydrocarbon receptor by structurally diverse exogenous and endogenous chemicals. Annu. Rev. Pharmacol. Toxicol. *43*, 309–334. https://doi.org/10.1146/annurev.pharmtox.43.100901.135828.

14. Poland, A., Glover, E., and Kende, A.S. (1976). Stereospecific, high affinity binding of 2,3,7,8-tetrachlorodibenzo-p-dioxin by hepatic cytosol. Evidence that the binding species is receptor for induction of aryl hydrocarbon hydroxylase. J. Biol. Chem. *251*, 4936–4946.

15. Bianchi-Smiraglia, A., Bagati, A., Fink, E.E., Affronti, H.C., Lipchick, B.C., Moparthy, S., Long, M.D., Rosario, S.R., Lightman, S.M., Moparthy, K., et al. (2018). Inhibition of the aryl hydrocarbon receptor/polyamine biosynthesis axis suppresses multiple myeloma. J. Clin. Invest. *128*, 4682–4696. https://doi.org/10.1172/JCI70712.

16. Opitz, C.A., Litzenburger, U.M., Sahm, F., Ott, M., Tritschler, I., Trump, S., Schumacher, T., Jestaedt, L., Schrenk, D., Weller, M., et al. (2011). An endogenous tumour-promoting ligand of the human aryl hydrocarbon receptor. Nature *478*, 197–203. https://doi.org/10.1038/nature10491.

17. Sadik, A., Somarribas Patterson, L.F., Öztürk, S., Mohapatra, S.R., Panitz, V., Secker, P.F., Pfänder, P., Loth, S., Salem, H., Prentzell, M.T., et al. (2020). IL4I1 Is a Metabolic Immune Checkpoint that Activates the AHR and Promotes Tumor Progression. Cell *182*, 1252–1270.e34. https://doi.org/10.1016/j.cell.2020.07.038.

18. Goode, G.D., Ballard, B.R., Manning, H.C., Freeman, M.L., Kang, Y., and Eltom, S.E. (2013). Knockdown of aberrantly upregulated aryl hydrocarbon receptor reduces tumor growth and metastasis of MDA-MB-231 human breast cancer cell line. International journal of cancer. Int. J. Cancer *133*, 2769–2780. https://doi.org/10.1002/ijc.28297.

19. Goode, G., Pratap, S., and Eltom, S.E. (2014). Depletion of the aryl hydrocarbon receptor in MDA-MB-231 human breast cancer cells altered the expression of genes in key regulatory pathways of cancer. PLoS One *9*, e100103. https://doi.org/10.1371/journal.pone.0100103.

20. Ide, H., Lu, Y., Yu, J., Noguchi, T., Kanayama, M., Muto, S., Yamaguchi, R., Kawato, S., and Horie, S. (2017). Aryl hydrocarbon receptor signaling involved in the invasiveness of LNCaP cells. Hum. Cell *30*, 133–139. https://doi.org/10.1007/s13577-016-0158-2.

21. Yang, X., Liu, D., Murray, T.J., Mitchell, G.C., Hesterman, E.V., Karchner, S.I., Merson, R.R., Hahn, M.E., and Sherr, D.H. (2005). The aryl hydrocarbon receptor constitutively represses c-myc transcription in human mammary tumor cells. Oncogene *24*, 7869–7881. https://doi.org/10.1038/sj.onc.1208938.

22. Fan, Y., Boivin, G.P., Knudsen, E.S., Nebert, D.W., Xia, Y., and Puga, A. (2010). The aryl hydrocarbon receptor functions as a tumor suppressor of liver carcinogenesis. Cancer Res. *70*, 212–220. https://doi.org/10.1158/0008-5472.CAN-09-3090.

23. Hanieh, H., Mohafez, O., Hairul-Islam, V.I., Alzahrani, A., Bani Ismail, M., and Thirugnanasambantham, K. (2016). Novel Aryl Hydrocarbon Receptor Agonist Suppresses Migration and Invasion of Breast Cancer Cells. PLoS One *11*, e0167650. https://doi.org/10.1371/journal.pone.0167650.

24. O'Donnell, E.F., Koch, D.C., Bisson, W.H., Jang, H.S., and Kolluri, S.K. (2014). The aryl hydrocarbon receptor mediates raloxifene-induced apoptosis in estrogen receptor-negative hepatoma and breast cancer cells. Cell Death Dis. *5*, e1038. https://doi.org/10.1038/cddis.2013.549.

25. Wu, P.Y., Liao, Y.F., Juan, H.F., Huang, H.C., Wang, B.J., Lu, Y.L., Yu, I.S., Shih, Y.Y., Jeng, Y.M., Hsu, W.M., and Lee, H. (2014). Aryl hydrocarbon receptor downregulates MYCN expression and promotes cell differentiation of neuroblastoma. PLoS One *9*, e88795. https://doi.org/10.1371/journal.pone.0088795.

26. Wu, P.Y., Yu, I.S., Lin, Y.C., Chang, Y.T., Chen, C.C., Lin, K.H., Tseng, T.H., Kargren, M., Tai, Y.L., Shen, T.L., et al. (2019). Activation of Aryl Hydrocarbon Receptor by Kynurenine Impairs Progression and Metastasis of Neuroblastoma. Cancer Res. *79*, 5550–5562. https://doi.org/10.1158/0008-5472.CAN-18-3272.

27. Jin, U.H., Karki, K., Cheng, Y., Michelhaugh, S.K., Mittal, S., and Safe, S. (2019). The aryl hydrocarbon receptor is a tumor suppressor-like gene in glioblastoma. J. Biol. Chem. *294*, 11342–11353. https://doi.org/10.1074/jbc.RA119.008882.

28. Murray, I.A., Patterson, A.D., and Perdew, G.H. (2014). Aryl hydrocarbon receptor ligands in cancer: friend and foe. Nat. Rev. Cancer *14*, 801–814. https://doi.org/10.1038/nrc3846.

29. Sherr, D.H., and Monti, S. (2013). The role of the aryl hydrocarbon receptor in normal and malignant B cell development. Semin. Immunopathol. *35*, 705–716. https://doi.org/10.1007/s00281-013-0390-8.

30. Kim, D.W., Gazourian, L., Quadri, S.A., Romieu-Mourez, R., Sherr, D.H., and Sonenshein, G.E. (2000). The RelA NF-kappaB subunit and the aryl hydrocarbon receptor (AhR) cooperate to transactivate the c-myc promoter in mammary cells. Oncogene *19*, 5498–5506. https://doi.org/10.1038/sj.onc.1203945.

31. Adler-Shohet, F.C., Singh, J., Nieves, D., Ashouri, N., Tran, M.T., Flores, M.C., and Arrieta, A. (2020). Safety and Tolerability of Clofazimine in a Cohort of Children With Odontogenic Mycobacterium abscessus Infection. J. Pediatric Infect. Dis. Soc. *9*, 483–485. https://doi.org/10.1093/jpids/piz049.

32. Cameron, L.H., Peloquin, C.A., Hiatt, P., Mann, M., Starke, J.R., Faircloth, J., McNeil, J.C., Patel, A., and Ruiz, F. (2022). Administration and monitoring of clofazimine for NTM infections in children with and without cystic fibrosis. J. Cyst.

Fibros. *21*, 348–352. https://doi.org/10.1016/j.jcf.2021.08.010.

33. Breit, S., and Schwab, M. (1989). Suppression of MYC by high expression of NMYC in human neuroblastoma cells. J. Neurosci. Res. *24*, 21–28. https://doi.org/10.1002/jnr.490240105.

34. Westermann, F., Muth, D., Benner, A., Bauer, T., Henrich, K.O., Oberthuer, A., Brors, B., Beissbarth, T., Vandesompele, J., Pattyn, F., et al. (2008). Distinct transcriptional MYCN/c-MYC activities are associated with spontaneous regression or malignant progression in neuroblastomas. Genome Biol. *9*, R150. https://doi.org/10.1186/gb-2008-9-10-r150.

35. Chen, L., Alexe, G., Dharia, N.V., Ross, L., Iniguez, A.B., Conway, A.S., Wang, E.J., Veschi, V., Lam, N., Qi, J., et al. (2018). CRISPR-Cas9 screen reveals a MYCN-amplified neuroblastoma dependency on EZH2. J. Clin. Invest. *128*, 446–462. https://doi.org/10.1172/JCI90793.

36. Wang, Z., Snyder, M., Kenison, J.E., Yang, K., Lara, B., Lydell, E., Bennani, K., Novikov, O., Federico, A., Monti, S., and Sherr, D.H. (2020). How the AHR Became Important in Cancer: The Role of Chronically Active AHR in Cancer Aggression. Int. J. Mol. Sci. *22*, 387. https://doi.org/10.3390/ijms22010387.

37. Jiang, H., Greathouse, R.L., Tiche, S.J., Zhao, M., He, B., Li, Y., Li, A.M., Forgo, B., Yip, M., Li, A., et al. (2023). Mitochondrial Uncoupling Induces Epigenome Remodeling and Promotes Differentiation in Neuroblastoma. Cancer Res. *83*, 181–194. https://doi.org/10.1158/0008-5472.CAN-22-1029.

38. Kim, S.H., Henry, E.C., Kim, D.K., Kim, Y.H., Shin, K.J., Han, M.S., Lee, T.G., Kang, J.K., Gasiewicz, T.A., Ryu, S.H., and Suh, P.G. (2006). Novel compound 2-methyl-2H-pyrazole-3-carboxylic acid (2-methyl-4-o-tolylazo-phenyl)-amide (CH-223191) prevents 2,3,7,8-TCDD-induced toxicity by antagonizing the aryl hydrocarbon receptor. Mol. Pharmacol. *69*, 1871–1878. https://doi.org/10.1124/mol.105.021832.

39. Campesato, L.F., Budhu, S., Tchaicha, J., Weng, C.H., Gigoux, M., Cohen, I.J., Redmond, D., Mangarin, L., Pourpe, S., Liu, C., et al. (2020). Blockade of the AHR restricts a Treg-macrophage suppressive axis induced by L-Kynurenine. Nat. Commun. *11*, 4011. https://doi.org/10.1038/s41467-020-17750-z.

40. Sung, P.J., Boulos, N., Tilby, M.J., Andrews, W.D., Newbold, R.F., Tweddle, D.A., and Lunec, J. (2013). Identification and characterisation of STMN4 and ROBO2 gene involvement in neuroblastoma cell differentiation. Cancer Lett. *328*, 168–175. https://doi.org/10.1016/j.canlet.2012.08.015.

41. Homman-Ludiye, J., Kwan, W.C., de Souza, M.J., Rodger, J., and Bourne, J.A. (2017). Ephrin-A2 regulates excitatory neuron differentiation and interneuron migration in the developing neocortex. Sci. Rep. *7*, 11813. https://doi.org/10.1038/s41598-017-12185-x.

42. Ferreira, A., and Caceres, A. (1992). Expression of the class III beta-tubulin isotype in developing neurons in culture. J. Neurosci. Res. *32*, 516–529. https://doi.org/10.1002/jnr.490320407.

43. Jiang, Y.Q., and Oblinger, M.M. (1992). Differential regulation of beta III and other tubulin genes during peripheral and central neuron development. J. Cell Sci. *103*, 643–651. https://doi.org/10.1242/jcs.103.3.643.

44. Gingras, M., Champigny, M.F., and Berthod, F. (2007). Differentiation of human adult skin-derived neuronal precursors into mature neurons. J. Cell. Physiol. *210*, 498–506. https://doi.org/10.1002/jcp.20889.

45. Hardwick, L.J.A., Ali, F.R., Azzarelli, R., and Philpott, A. (2015). Cell cycle regulation of proliferation versus differentiation in the central nervous system. Cell Tissue Res. *359*, 187–200. https://doi.org/10.1007/s00441-014-1895-8.

46. Kang, J.H., Rychahou, P.G., Ishola, T.A., Qiao, J., Evers, B.M., and Chung, D.H. (2006). MYCN silencing induces differentiation and apoptosis in human neuroblastoma cells. Biochem. Biophys. Res. Commun. *351*, 192–197. https://doi.org/10.1016/j.bbrc.2006.10.020.

47. Slack, A., Chen, Z., Tonelli, R., Pule, M., Hunt, L., Pession, A., and Shohet, J.M. (2005). The p53 regulatory gene MDM2 is a direct transcriptional target of MYCN in neuroblastoma. Proc. Natl. Acad. Sci. USA *102*, 731–736. https://doi.org/10.1073/pnas.0405495102.

48. Raetz, E.A., Kim, M.K.H., Moos, P., Carlson, M., Bruggers, C., Hooper, D.K., Foot, L., Liu, T., Seeger, R., and Carroll, W.L. (2003). Identification of genes that are regulated transcriptionally by Myc in childhood tumors. Cancer *98*, 841–853. https://doi.org/10.1002/cncr.11584.

49. Chen, T., and Dent, S.Y.R. (2014). Chromatin modifiers and remodellers: regulators of cellular differentiation. Nat. Rev. Genet. *15*, 93–106. https://doi.org/10.1038/nrg3607.

50. Ernst, J., and Kellis, M. (2012). ChromHMM: automating chromatin-state discovery and characterization. Nat. Methods *9*, 215–216. https://doi.org/10.1038/nmeth.1906.

51. Upton, K., Modi, A., Patel, K., Kendsersky, N.M., Conkrite, K.L., Sussman, R.T., Way, G.P., Adams, R.N., Sacks, G.I., Fortina, P., et al. (2020). Epigenomic profiling of neuroblastoma cell lines. Sci. Data *7*, 116. https://doi.org/10.1038/s41597-020-0458-y.

52. Sengupta, S., and George, R.E. (2017). Super-Enhancer-Driven Transcriptional Dependencies in Cancer. Trends Cancer *3*, 269–281. https://doi.org/10.1016/j.trecan.2017.03.006.

53. van Groningen, T., Koster, J., Valentijn, L.J., Zwijnenburg, D.A., Akogul, N., Hasselt, N.E., Broekmans, M., Haneveld, F., Nowakowska, N.E., Bras, J., et al. (2017). Neuroblastoma is composed of two super-enhancer-associated differentiation states. Nat. Genet. *49*, 1261–1266. https://doi.org/10.1038/ng.3899.

54. Whyte, W.A., Orlando, D.A., Hnisz, D., Abraham, B.J., Lin, C.Y., Kagey, M.H., Rahl, P.B., Lee, T.I., and Young, R.A. (2013). Master transcription factors and mediator establish super-enhancers at key cell identity genes. Cell *153*, 307–319. https://doi.org/10.1016/j.cell.2013.03.035.

55. Boeva, V., Louis-Brennetot, C., Peltier, A., Durand, S., Pierre-Eugène, C., Raynal, V., Etchevers, H.C., Thomas, S., Lermine, A., Daudigeos-Dubus, E., et al. (2017). Heterogeneity of neuroblastoma cell identity defined by transcriptional circuitries. Nat. Genet. *49*, 1408–1413. https://doi.org/10.1038/ng.3921.

56. Pei, D., Luther, W., Wang, W., Paw, B.H., Stewart, R.A., and George, R.E. (2013).

Distinct neuroblastoma-associated alterations of PHOX2B impair sympathetic neuronal differentiation in zebrafish models. PLoS Genet. *9*, e1003533. https://doi.org/10.1371/journal.pgen.1003533.

57. Lu, J., Tan, L., Li, P., Gao, H., Fang, B., Ye, S., Geng, Z., Zheng, P., and Song, H. (2009). All-trans retinoic acid promotes neural lineage entry by pluripotent embryonic stem cells via multiple pathways. BMC Cell Biol. *10*, 57. https://doi.org/10.1186/1471-2121-10-57.

58. Sainero-Alcolado, L., Mushtaq, M., Liaño-Pons, J., Rodriguez-Garcia, A., Yuan, Y., Liu, T., Ruiz-Pérez, M.V., Schlisio, S., Bedoya-Reina, O., and Arsenian-Henriksson, M. (2022). Expression and activation of nuclear hormone receptors result in neuronal differentiation and favorable prognosis in neuroblastoma. J. Exp. Clin. Cancer Res. *41*, 226. https://doi.org/10.1186/s13046-022-02399-x.

59. Muley, P.D., McNeill, E.M., Marzinke, M.A., Knobel, K.M., Barr, M.M., and Clagett-Dame, M. (2008). The atRA-responsive gene neuron navigator 2 functions in neurite outgrowth and axonal elongation. Dev. Neurobiol. *68*, 1441–1453. https://doi.org/10.1002/dneu.20670.

60. Duffy, D.J., Krstic, A., Halasz, M., Schwarzl, T., Konietzny, A., Iljin, K., Higgins, D.G., and Kolch, W. (2017). Retinoic acid and TGF-beta signalling cooperate to overcome MYCN-induced retinoid resistance. Genome Med. *9*, 15. https://doi.org/10.1186/s13073-017-0407-3.

61. Abemayor, E., Chang, B., and Sidell, N. (1990). Effects of retinoic acid on the in vivo growth of human neuroblastoma cells. Cancer Lett. *55*, 1–5. https://doi.org/10.1016/0304-3835(90)90057-5.

62. Juricek, L., and Coumoul, X. (2018). The Aryl Hydrocarbon Receptor and the Nervous System. Int. J. Mol. Sci. *19*, 2504. https://doi.org/10.3390/ijms19092504.

63. Akahoshi, E., Yoshimura, S., and Ishihara-Sugano, M. (2006). Over-expression of AhR (aryl hydrocarbon receptor) induces neural differentiation of Neuro2a cells: neurotoxicology study. Environ. Health. *5*, 24. https://doi.org/10.1186/1476-069X-5-24.

64. Huang, T.C., Chang, H.Y., Chen, C.Y., Wu, P.Y., Lee, H., Liao, Y.F., Hsu, W.M., Huang, H.C., and Juan, H.F. (2011). Silencing of miR-124 induces neuroblastoma SK-N-SH cell differentiation, cell cycle arrest and apoptosis through promoting AHR. FEBS Lett. *585*, 3582–3586. https://doi.org/10.1016/j.febslet.2011.10.025.

65. Karasová, M., Procházková, J., Tylichová, Z., Fedr, R., Ciganek, M., Machala, M., Dvořák, Z., Vyhlídalová, B., Zůvalová, I., Ehrmann, J., et al. (2022). Inhibition of Aryl Hydrocarbon Receptor (AhR) Expression Disrupts Cell Proliferation and Alters Energy Metabolism and Fatty Acid Synthesis in Colon Cancer Cells. Cancers *14*, 4245. https://doi.org/10.3390/cancers14174245.

66. Xu, T., Luo, Y., Xie, H.Q., Xia, Y., Li, Y., Chen, Y., Guo, Z., Xu, L., and Zhao, B. (2022). Systematic identification of molecular mechanisms for aryl hydrocarbon receptor mediated neuroblastoma cell migration. Environ. Int. *168*, 107461. https://doi.org/10.1016/j.envint.2022.107461.

67. Kerr, M.A., Nasca, P.C., Mundt, K.A., Michalek, A.M., Baptiste, M.S., and Mahoney, M.C. (2000). Parental occupational exposures and risk of neuroblastoma: a case-control study

(United States). Cancer Causes Control. *11*, 635–643. https://doi.org/10.1023/a:1008951632482.

68. Watanabe, K., Yamaji, R., and Ohtsuki, T. (2018). MicroRNA-664a-5p promotes neuronal differentiation of SH-SY5Y cells. Gene Cell. *23*, 225–233. https://doi.org/10.1111/gtc.12559.

69. Imran, S., Ferretti, P., and Vrzal, R. (2015). Different regulation of aryl hydrocarbon receptor-regulated genes in response to dioxin in undifferentiated and neuronally differentiated human neuroblastoma SH-SY5Y cells. Toxicol. Mech. Methods *25*, 689–697. https://doi.org/10.3109/15376516.2015.1070227.

70. Safe, S., and Zhang, L. (2022). The Role of the Aryl Hydrocarbon Receptor (AhR) and Its Ligands in Breast Cancer. Cancers *14*, 5574. https://doi.org/10.3390/cancers14225574.

71. Cano-Sanchez, J., Murillo-Gonzalez, F.E., de Jesus-Aguilar, J., Cabanas-Cortes, M.A., Tirado-Garibay, A.C., and Elizondo, G. (2023). The Aryl Hydrocarbon Receptor Ligand 6-Formylindolo(3,2-b)carbazole Promotes Estrogen Receptor Alpha and c-Fos Protein Degradation and Inhibits MCF-7 Cell Proliferation and Migration. Pharmacology *108*, 157–165. https://doi.org/10.1159/000527993.

72. Wu, P.Y., Chuang, P.Y., Chang, G.D., Chan, Y.Y., Tsai, T.C., Wang, B.J., Lin, K.H., Hsu, W.M., Liao, Y.F., and Lee, H. (2019). Novel Endogenous Ligands of Aryl Hydrocarbon Receptor Mediate Neural Development and Differentiation of Neuroblastoma. ACS Chem. Neurosci. *10*, 4031–4042. https://doi.org/10.1021/acschemneuro.9b00273.

73. Fritz, W.A., Lin, T.M., Cardiff, R.D., and Peterson, R.E. (2007). The aryl hydrocarbon receptor inhibits prostate carcinogenesis in TRAMP mice. Carcinogenesis *28*, 497–505. https://doi.org/10.1093/carcin/bgl179.

74. Han, H., Davidson, L.A., Hensel, M., Yoon, G., Landrock, K., Allred, C., Jayaraman, A., Ivanov, I., Safe, S.H., and Chapkin, R.S. (2021). Loss of Aryl Hydrocarbon Receptor Promotes Colon Tumorigenesis in Apc(S580/+); Kras(G12D/+) Mice. Mol. Cancer Res. *19*, 771–783. https://doi.org/10.1158/1541-7786.MCR-20-0789.

75. Ghotbaddini, M., Moultrie, V., and Powell, J.B. (2018). Constitutive Aryl Hydrocarbon Receptor Signaling in Prostate Cancer Progression. J. Cancer Treatment Diagn. *2*, 11–16. https://doi.org/10.29245/2578-2967/2018/5.1136.

76. Papoutsis, A.J., Selmin, O.I., Borg, J.L., and Romagnolo, D.F. (2015). Gestational exposure to the AhR agonist 2,3,7,8-tetrachlorodibenzo-p-dioxin induces BRCA-1 promoter hypermethylation and reduces BRCA-1 expression in mammary tissue of rat offspring: preventive effects of resveratrol. Mol. Carcinog. *54*, 261–269. https://doi.org/10.1002/mc.22095.

77. Frauenstein, K., Sydlik, U., Tigges, J., Majora, M., Wiek, C., Hanenberg, H., Abel, J., Esser, C., Fritsche, E., Krutmann, J., and Haarmann-Stemmann, T. (2013). Evidence for a novel anti-apoptotic pathway in human keratinocytes involving the aryl hydrocarbon receptor, E2F1, and checkpoint kinase 1. Cell Death Differ. *20*, 1425–1434. https://doi.org/10.1038/cdd.2013.102.

78. Mulero-Navarro, S., and Fernandez-Salguero, P.M. (2016). New Trends in Aryl Hydrocarbon Receptor Biology. Front. Cell Dev. Biol. *4*, 45. https://doi.org/10.3389/fcell.2016.00045.

79. Nguyen, T.A., Hoivik, D., Lee, J.E., and Safe, S. (1999). Interactions of nuclear receptor coactivator/corepressor proteins with the aryl hydrocarbon receptor complex. Arch. Biochem. Biophys. *367*, 250–257. https://doi.org/10.1006/abbi.1999.1282.

80. Rohrer, H. (2011). Transcriptional control of differentiation and neurogenesis in autonomic ganglia. Eur. J. Neurosci. *34*, 1563–1573. https://doi.org/10.1111/j.1460-9568.2011.07860.x.

81. Pattyn, A., Morin, X., Cremer, H., Goridis, C., and Brunet, J.F. (1999). The homeobox gene Phox2b is essential for the development of autonomic neural crest derivatives. Nature *399*, 366–370. https://doi.org/10.1038/20700.

82. Almutairi, B., Charlet, J., Dallosso, A.R., Szemes, M., Etchevers, H.C., Malik, K.T.A., and Brown, K.W. (2019). Epigenetic deregulation of GATA3 in neuroblastoma is associated with increased GATA3 protein expression and with poor outcomes. Sci. Rep. *9*, 18934. https://doi.org/10.1038/s41598-019-55382-6.

83. Bachetti, T., Di Paolo, D., Di Lascio, S., Mirisola, V., Brignole, C., Bellotti, M., Caffa, I., Ferraris, C., Fiore, M., Fornasari, D., et al. (2010). PHOX2B-mediated regulation of ALK expression: in vitro identification of a functional relationship between two genes involved in neuroblastoma. PLoS One *5*, e13108. https://doi.org/10.1371/journal.pone.0013108.

84. Viprey, V.F., Gregory, W.M., Corrias, M.V., Tchirkov, A., Swerts, K., Vicha, A., Dallorso, S., Brock, P., Luksch, R., Valteau-Couanet, D., et al. (2014). Neuroblastoma mRNAs predict outcome in children with stage 4 neuroblastoma: a European HR-NBL1/SIOPEN study. J. Clin. Oncol. *32*, 1074–1083. https://doi.org/10.1200/JCO.2013.53.3604.

85. Zimmerman, M.W., Durbin, A.D., He, S., Oppel, F., Shi, H., Tao, T., Li, Z., Berezovskaya, A., Liu, Y., Zhang, J., et al. (2021). Retinoic acid rewires the adrenergic core regulatory circuitry of childhood neuroblastoma. Sci. Adv. *7*, eabe0834. https://doi.org/10.1126/sciadv.abe0834.

86. Mandavia, C. (2015). TCDD-induced activation of aryl hydrocarbon receptor regulates the skin stem cell population. Med. Hypotheses *84*, 204–208. https://doi.org/10.1016/j.mehy.2014.12.023.

87. Dever, D.P., and Opanashuk, L.A. (2012). The aryl hydrocarbon receptor contributes to the proliferation of human medulloblastoma cells. Mol. Pharmacol. *81*, 669–678. https://doi.org/10.1124/mol.111.077305.

88. Lafita-Navarro, M.C., Kim, M., Borenstein-Auerbach, N., Venkateswaran, N., Hao, Y.H., Ray, R., Brabletz, T., Scaglioni, P.P., Shay, J.W., and Conacci-Sorrell, M. (2018). The aryl hydrocarbon receptor regulates nucleolar activity and protein synthesis in MYC-expressing cells. Genes Dev. *32*, 1303–1308. https://doi.org/10.1101/gad.313007.118.

89. Lafita-Navarro, M.C., Perez-Castro, L., Zacharias, L.G., Barnes, S., DeBerardinis, R.J., and Conacci-Sorrell, M. (2020). The transcription factors aryl hydrocarbon receptor and MYC cooperate in the regulation of cellular metabolism. J. Biol. Chem. *295*, 12398–12407. https://doi.org/10.1074/jbc.AC120.014189.

90. Reynolds, C.P., Matthay, K.K., Villablanca, J.G., and Maurer, B.J. (2003). Retinoid therapy of high-risk neuroblastoma. Cancer Lett. *197*, 185–192. https://doi.org/10.1016/s0304-3835(03)00108-3.

91. Gopal, M., Padayatchi, N., Metcalfe, J.Z., and O'Donnell, M.R. (2013). Systematic review of clofazimine for the treatment of drug-resistant tuberculosis. Int. J. Tuberc. Lung Dis. *17*, 1001–1007. https://doi.org/10.5588/ijtld.12.0144.

92. Smith, C.S., Aerts, A., Saunderson, P., Kawuma, J., Kita, E., and Virmond, M. (2017). Multidrug therapy for leprosy: a game changer on the path to elimination. Lancet Infect. Dis. *17*, e293–e297. https://doi.org/10.1016/S1473-3099(17)30418-8.

93. Mor, A., Tankiewicz-Kwedlo, A., and Pawlak, D. (2021). Kynurenines as a Novel Target for the Treatment of Malignancies. Pharmaceuticals *14*, 606. https://doi.org/10.3390/ph14070606.

94. Dobin, A., Davis, C.A., Schlesinger, F., Drenkow, J., Zaleski, C., Jha, S., Batut, P., Chaisson, M., and Gingeras, T.R. (2013). STAR: ultrafast universal RNA-seq aligner. Bioinformatics *29*, 15–21. https://doi.org/10.1093/bioinformatics/bts635.

95. Love, M.I., Huber, W., and Anders, S. (2014). Moderated estimation of fold change and dispersion for RNA-seq data with DESeq2. Genome Biol. *15*, 550. https://doi.org/10.1186/s13059-014-0550-8.

96. Reimand, J., Isserlin, R., Voisin, V., Kucera, M., Tannus-Lopes, C., Rostamianfar, A., Wadi, L., Meyer, M., Wong, J., Xu, C., et al. (2019). Pathway enrichment analysis and visualization of omics data using g:Profiler, GSEA, Cytoscape and EnrichmentMap. Nat. Protoc. *14*, 482–517. https://doi.org/10.1038/s41596-018-0103-9.

97. Liberzon, A., Subramanian, A., Pinchback, R., Thorvaldsdóttir, H., Tamayo, P., and Mesirov, J.P. (2011). Molecular signatures database (MSigDB) 3.0. Bioinformatics *27*, 1739–1740. https://doi.org/10.1093/bioinformatics/btr260.

98. Hänzelmann, S., Castelo, R., and Guinney, J. (2013). GSVA: gene set variation analysis for microarray and RNA-seq data. BMC Bioinf. *14*, 7. https://doi.org/10.1186/1471-2105-14-7.

99. Buenrostro, J.D., Wu, B., Chang, H.Y., and Greenleaf, W.J. (2015). ATAC-seq: A Method for Assaying Chromatin Accessibility Genome-Wide. Curr. Protoc. Mol. Biol. *109*, 21.29.1–21.29.9. https://doi.org/10.1002/0471142727.mb2129s109.

100. Zhang, Y., Liu, T., Meyer, C.A., Eeckhoute, J., Johnson, D.S., Bernstein, B.E., Nusbaum, C., Myers, R.M., Brown, M., Li, W., and Liu, X.S. (2008). Model-based analysis of ChIP-Seq (MACS). Genome Biol. *9*, R137. https://doi.org/10.1186/gb-2008-9-9-r137.

101. Stark, R.B. (2011). DiffBind: Differential Binding Analysis of ChIP-Seq Peak Data (Bioconductor).

102. Layer, R.M., Pedersen, B.S., DiSera, T., Marth, G.T., Gertz, J., and Quinlan, A.R. (2018). GIGGLE: a search engine for large-scale integrated genome analysis. Nat. Methods *15*, 123–126. https://doi.org/10.1038/nmeth.4556.

103. Mei, S., Qin, Q., Wu, Q., Sun, H., Zheng, R., Zang, C., Zhu, M., Wu, J., Shi, X., Taing, L., et al. (2017). Cistrome Data Browser: a data portal for ChIP-Seq and chromatin accessibility data in human and mouse. Nucleic Acids Res. *45*, D658–D662. https://doi.org/10.1093/nar/gkw983.

104. Long, M.D., Jacobi, J.J., Singh, P.K., Llimos, G., Wani, S.A., Rowsam, A.M., Rosario, S.R., Hoogstraat, M., Linder, S., Kirk, J., et al.

(2021). Reduced NCOR2 expression accelerates androgen deprivation therapy failure in prostate cancer. Cell Rep. *37*, 110109. https://doi.org/10.1016/j.celrep.2021.110109.

105. Lawrence, M., Huber, W., Pagès, H., Aboyoun, P., Carlson, M., Gentleman, R., Morgan, M.T., and Carey, V.J. (2013). Software for computing and annotating genomic ranges. PLoS Comput. Biol. *9*, e1003118. https://doi.org/10.1371/journal.pcbi.1003118.

106. Bianchi-Smiraglia, A., Wolff, D.W., Marston, D.J., Deng, Z., Han, Z., Moparthy, S., Wombacher, R.M., Mussell, A.L., Shen, S., Chen, J., et al. (2021). Regulation of local GTP availability controls RAC1 activity and cell invasion. Nat. Commun. *12*, 6091. https://doi.org/10.1038/s41467-021-26324-6.

107. Pemberton, K., Mersman, B., and Xu, F. (2018). Using ImageJ to Assess Neurite Outgrowth in Mammalian Cell Cultures: Research Data Quantification Exercises in Undergraduate Neuroscience Lab. J. Undergrad. Neurosci. Educ. *16*, A186–A194.

STAR★METHODS

KEY RESOURCES TABLE

REAGENT or RESOURCE	SOURCE	IDENTIFIER
Antibodies		
Rabbit monoclonal to MycN (D1V2A)	Cell Signaling	Cat# 84406, RRID:AB_2800038
Rabbit monoclonal to AhR (D5S6H)	Cell Signaling	Cat# 83200, RRID:AB_2800011
Rabbit polyclonal to c-Myc	Cell Signaling	Cat# 9402, RRID:AB_2151827
Rabbit monoclonal to beta-tubulin-III (D71G9)	Cell Signaling	Cat# 5568, RRID:AB_10694505
Rabbit polyclonal to neurofilament-L (C28E10)	Cell Signaling	Cat# 2837, RRID:AB_823575
Mouse monoclonal to AhR (A-3)	Santa Cruz Biotechnology	Cat# sc-133088, RRID:AB_2273721
Mouse monoclonal to alpha-tubulin (B-5-1-2)	Sigma Aldrich	Cat# T6074, RRID:AB_477582
HRP-beta actin	Proteintech	HRP-60008, RRID:AB_2819183
HRP-GAPDH	Proteintech	Cat# HRP-60004, RRID:AB_2737588
Alexa Fluor 568 (Red) -conjugated goat-*anti*-rabbit antibody	Thermo Fisher Scientific	Cat# A21069, RRID:AB_1056360
Chemicals, peptides, and recombinant proteins		
Alexa Fluor 488 (Green)-conjugated phalloidin	Thermo Fisher Scientific	Cat# A12379
Hoechst-33342	Invitrogen	Cat#H3570
Clofazimine	Sigma Aldrich	Cat#C8895
CH-223191	Sigma Aldrich	Cat#C8124
all-trans-retinoic acid (ATRA)	Sigma Aldrich	Cat#R2625
BAY-2416964	Selleckchem	Cat#S8995
KYN-101	Aobious	Cat# AOB11039
LipoD293	SignaGen	Cat# SL100668
Hexadimethrine bromide	Sigma Aldrich	Cat#H9268
PureLink DNase Set	Thermo Fisher Scientific	Cat#12185010
Critical commercial assays		
PureLink RNA Mini kit	Thermo Fisher Scientific	Cat#12183018A
High-Capacity cDNA Reverse Transcription kit	Thermo Fisher Scientific	Cat# 4368814
Hema3 Staining Kit	Fisher Scientific	Cat#22-123869
8.0 μm Biocoat Matrigel-Coated Invasion Chambers	Corning	Cat#354480
Deposited data		
RNAseq	This Paper	GEO; GSE224037
ATACseq	This Paper	GEO:GSE224390
GSE224037 + GSE224390	This Paper	GEO Super-Series: GSE224391
Experimental models: Cell lines		
Human *MYCN*-amplified neuroblastoma Kelly	Dr. Katerina Gurova	N/A
Human *MYCN*-amplified neuroblastoma BE2C	Dr. Katerina Gurova	N/A
Human *MYCN*-amplified neuroblastoma IMR-32	Dr. Michael Higgins	N/A
Human non-*MYCN*-amplified neuroblastoma SK-N-SH	Dr. Michael Higgins	N/A
Human non-*MYCN*-amplified neuroblastoma SH-SY5Y	Dr. Michael Higgins	N/A
Human non-*MYCN*-amplified neuroblastoma SHEP	Dr. Michelle Haber	N/A
Human non-*MYCN*-amplified neuroblastoma NBL-S	Dr. Michelle Haber	N/A
HEK293-T	Dr. Irwin Gelman	N/A

Continued

REAGENT or RESOURCE	SOURCE	IDENTIFIER
Experimental models: Organisms/strains		
Mouse: NOD-SCID Gamma (NSG)	Roswell Park Comprehensive Cancer Center Colony	N/A
Oligonucleotides		
siRNA pools against MYCN	Santa Cruz Biotechnology	Cat#sc-36003
Primer for MYCN amplification qRT-PCR_FWD 5′ CACAAGGCCCTCAGTACCTC 3′	This Paper	N/A
Primer for MYCN amplification qRT-PCR_REV 5′ ACCACGTCGATTTCTTCCTC 3′	This Paper	N/A
Primer for RPS20 amplification qRT-PCR_FWD 5′ AAGGATACCGGAAAAACACCC 3′	This Paper	N/A
Primer for RPS20 amplification qRT-PCR_REV 5′ TTTACGTTGCGGCTTGTTAGG 3′	This Paper	N/A
Recombinant DNA		
pLVp-SV4-puro lentiviral vector	Dr. Peter Chumakov	N/A
pLKO-GFP lentiviral vector	Sigma Aldrich	SHC005
pLKO-shAHR #1 lentiviral vector	Sigma Aldrich	TRCN0000245285
pLKO-shAHR#2 lentiviral vector	Sigma Aldrich	TRCN000021258
pCMV-VSV-G	Stewart et al. RNA (2003) Apr; 9(4):493-501	Addgene Plasmid # 8454
pCMV-psPAX2	Dr. Irwin Gelman	N/A
Software and algorithms		
ImageJ		https://imagej.nih.gov/ij/index.html
R v3.6–4.0	https://www.r-project.org/	https://www.r-project.org/
DESeq2	Love et al.[65]	https://bioconductor.org/packages/release/bioc/html/DESeq2.html
Bowtie2	Zhang et al.[70]	
DiffBind	Stark et al.[71]	
GIGGLE	Layer et al.[72]	
CistromeDB	Mei et al.[73]	
ChromHMM	Ernst et al.[38]	
GenomicRanges	Lawrence et al.[75]	
ROSE	Whyte et al.[42]	http://younglab.wi.mit.edu/super_enhancer_code.html
HOMER v4.11		http://homer.ucsd.edu/homer/
Graphpad Prism V9.3.1	Graphpad Software	https://www.graphpad.com/
ModFit	ModFit LT 5.0 software	
QuantStudio Real-Time PCR Software v1.3	Applied Biosystems	https://www.thermofisher.com/us/en/home/global/forms/life-science/quantstudio-6-7-flex-software.html
GeneSys	Syngene	https://www.syngene.com/software/genesys-rapid-gel-image-capture/
CompuSyn		https://www.combosyn.com/
R2: Genomics Analysis and Visualization Platform	Genomics Analysis and Visualization Platform (http://r2.amc.nl)	http://r2.amc.nl

RESOURCE AVAILABILITY

Lead contact

- Further information and requests for resources and reagents should be directed to and will be fulfilled by the lead contacts, Anna Bianchi-Smiraglia (Anna.Bianchi-Smiraglia@RoswellPark.org).

Materials availability

- This study did not generate new unique reagents.

Data and code availability

- All sequencing data reported here (RNAseq and ATACseq) are available in the NCBI Gene Expression Omnibus (GEO) database and are publicly available as of the date of publication. Accession numbers are listed in the key resources table.
- This paper does not report original code.
- Any additional information required to reanalyze the data reported in this paper is available from the lead contacts upon request.

EXPERIMENTAL MODEL AND STUDY PARTICIPANT DETAILS

Mouse models

All experiments involving animals were approved by the Institutional Animal Care and Use Committee. (IACUC) and listed under protocol 1450M. Kelly or BE2C cells (1×10^6) with indicated manipulations were resuspended in 100 μ L of Matrigel (Corning, Corning, NY, USA) and inoculated subcutaneously into the right flank of equal numbers of males and females 6-8-week-old NOD-SCID Gamma mice, bred and housed at the Division of Laboratory Animal Resources (Roswell Park Comprehensive Cancer Center, Buffalo, NY, USA). As neuroblastoma affects almost equally males and females (1.2:1 ratio) equal numbers of male and female mice were used. No sex difference emerged during the studies. Tumor volumes were recorded twice/week and mice were humanely euthanized when a tumor volume reached 2 cm^3 or when a tumor became ulcerated. No animals were excluded from the study since all animals developed palpable tumors within 2 weeks of subcutaneous inoculation of cells and no animals developed significant morbidity before the end of the study.

Cell lines

MYCN-amplified Kelly (female) and BE2C (male) cells were a kind gift from Dr. Katerina Gurova (Roswell Park Comprehensive Cancer Center, Buffalo, NY, USA). *MYCN*-amplified IMR32 (male) cells and non-*MYCN*-amplified SK-N-SH (female) and SH-SY5Y (female) cells were a kind gift from Dr. Michael Higgins (Roswell Park Comprehensive Cancer Center, Buffalo, NY, USA). Non-*MYCN*-amplified SHEP (female) and NBL-S (male) cells were a kind gift from Drs. Michelle Haber and Murray Norris (Children's Cancer Institute, Sydney, Australia). HEK-293T cells were a kind gift from Dr. Irwin Gelman (Roswell Park Comprehensive Cancer Center, Buffalo, NY, USA). Kelly, BE2C, and IMR32 cells were cultured in RPMI media (Invitrogen, Carlsbad, CA, USA); SK-N-SH, SH-SY5Y, SHEP, NBL-S, and HEK293T were cultured in DMEM media (Invitrogen). Both media were supplemented with 10% fetal bovine serum (Invitrogen) and antibiotic-antimycotic (Invitrogen). All cell lines were authenticated via short tandem repeat sequencing at the Roswell Park Genomics Shared Resource between November 2019 and March 2023 and routinely tested for mycoplasma contamination.

METHOD DETAILS

Lentiviral infections

Transfection of plasmids was performed using LipoD293 (SignaGen, Frederick, MD, USA) into HEK293T cells along with the pCMV-VSV-G vector (Addgene, Cambridge, MA, USA) and the pCMV-psPAX2 vector (a kind gift from Dr. Irwin Gelman, Roswell Park Comprehensive Cancer Center, Buffalo, NY, USA). The pLVp-SV4-puro lentiviral vector was obtained from Dr. Peter Chumakov (Cleveland Clinic, Cleveland, OH, USA). pLKO-GFP and shRNA toward AhR were purchased from Sigma: shAhR #1 TRCN0000245285; shAhR #2 TRCN000021258.

All lentiviral infections were performed as previously described.[15] Briefly, HEK293T cells were transfected with LipoD293 and target plasmid in the presence of packaging plasmids according to the manufacturer's protocol. The media was refreshed after 8hrs and lentiviral supernatant was harvested at 48hrs, filtered with a 0.45 μm filter and syringe, and transduced to cells in the presence of 8 μ g/mL hexadimethrine bromide (Sigma, St. Louis, MO, USA).

Cell cycle analysis

Approximately 2×10^6 cells were washed with PBS, harvested, and fixed in ice-cold 70% ethanol. Cells were washed twice with PBS, resuspended in staining buffer (100 mM Tris pH 7.4, 150 mM NaCl, 1 mM CaCl$_2$, 0.5 mM MgCl$_2$, 0.1% Nonidet P-40) with RNase A (10 μ g/mL), and incubated at 37°C for 30 min. Cells were resuspended in fresh staining buffer with propidium iodide solution (1 μ g/mL). Samples were acquired on an LSR Fortessa Becton Dickinson flow cytometry analyzer at the Roswell Park Comprehensive Cancer Center Flow & Image

Cytometry Shared Resource Facility using a 535/617 nm filter. Cell cycle analysis was conducted using ModFit LT 5.0 software (Verity Software House, Topsham, ME, USA).

Immunofluorescence

Immunofluorescence staining was performed as previously described.[15] Briefly, cells were grown on glass coverslips, fixed in 4% paraformaldehyde (PFA) in PBS, permeabilized in 0.01% Triton X-100 in PBS and blocked in 3% milk in PBS. Primary antibody incubation was carried out in 1% milk in PBS at room temperature, and secondary antibody and phalloidin staining were carried out in 0.5% milk in PBS at RT. Nuclei were stained with Hoechst 33258. Images were acquired with a Zeiss Axio Observer z.1 inverted microscope equipped a Zeiss Mrm camera and AxioVision 4.8 software.

RNA-seq

Total cellular RNA was isolated using the PureLink RNA Mini kit with on-column DNase treatment (Thermo Fisher Scientific). Sequencing libraries were prepared with the TruSeq Stranded mRNA kit (Illumina) from 500 ng total RNA following manufacturer's instructions. PCR-amplified libraries were pooled in an equimolar fashion, loaded into a 75-cycle NextSeq Reagent Cartridge, and single-end sequencing performed on a NextSeq 500 (Illumina) following the manufacturer's recommended protocol. Genome alignments and feature counting were performed at the Roswell Park Comprehensive Cancer Center's Genomics Shared Resource. Raw reads were mapped to the human reference genome (GRCh38.p13) using STAR.[94] Raw feature count normalization and differential expression analysis were carried out using DESeq2.[95] Differential expression rank order was used for subsequent GSEA,[96] performed using the cluster profile package in R. Gene sets queried included the Hallmark, Canonical pathways, and GO Biological Processes Ontology collections available through the Molecular Signatures Database (MSigDB).[97] For select pathways, per sample enrichment was calculated via ssGSEA, performed using the GSVA package.[98] Overlaps of DEG lists across companions were calculated by hypergeometric testing. All analyses were performed using R statistical software, version 4.1.1.

ATAC-seq

Samples for ATAC-seq were prepared using a protocol by Buenrostro et al.,[99] with minor modifications. Briefly, cells (5×10^3) in triplicates were collected in cold PBS and spun down. Pellets were gently resuspended in 50μL cold lysis buffer and nuclei were spun at 2,100 rpm, 10 min at 4°C. Supernatant was discarded and pellets were placed on ice for the transposition reaction. ATAC-seq libraries were prepared by incubating nuclei pellets with TD 2x buffer and TDE1 transposase by Illumina for 30 min at 37°C, followed by sample purification with Qiagen MinElute PCR purification kit. Transposed DNA fragments were amplified with 10 PCR cycles using a PCR primer (Ad1_noMX,IDT) and a barcoded PCR primer (Ad_index primer, IDT) with a NEB Next High Fidelity 2x PCR Master Mix (NEB). Libraries were sequenced with an Illumina NextSeq 500 Platform with 75 bps paired-end reads. Reads were aligned to the human (hg19) reference genome with Bowtie2 tool and called peaks using MACS3.[100] DARs were determined using DiffBind.[101] To find potential transcription factor binding enrichment within DARs, we utilized GIGGLE[102] to query the complete human transcription factor ChIP-seq dataset collection in Cistrome DB.[103] Putative co-enriched factors were identified by assessment of the number of time a given factor was observed in the top 200 most enriched datasets relative to the total number of datasets for that factor in the complete Cistrome DB (>1.2 FC enrichment over background).

ChromHMM

Previously published ChIP-seq data from Kelly cells (GSE138314)[51] was reprocessed and reanalyzed as previously detailed.[104] We applied ChromHMM[50] to learn the regulatory chromatin states in Kelly cells using the histone marks H3K4me1 (enhancer region), H3K4me3 (promoter region), H3K27me3 (repressive state), and H3K27ac (active state). We produced a new 13-chromatin state model which was further collapsed into 6 broad regulatory chromatin states based on histone mark signal intensity, human genomic region annotations, and TSS genomic neighborhoods: Quiescent/No Signal, Repressed/Polycomb (defined by H3K27me3), Bivalent/Poised Enhancer (defined by distal H3K4me1 and H3K27me3), Bivalent/Poised Promoter (defined by proximal H3K4me3 and H3K27me3), Active Enhancer (defined by distal H3K4me1 and H3K27ac), and Active Promoter (defined by proximal H3K4me3 and H3K27ac). Enrichment of ATAC-seq peaks within Kelly ChromHMM-defined regulatory states was performed using *GenomicRanges*[105] with a max overlap of 200 bp. Enrichment was defined as the percentage of overlapping regions proportional to the total genomic space defined in Kelly cells. All analyses were undertaken using the R platform for statistical computing (version 4.1 or later) using library packages implemented in *Bioconductor* or using the indicated software packages implemented in Java>1.6 and Python3.

Super-enhancers identification

Using the same reprocessed and reanalyzed ChIP-seq data from Kelly cells (GSE138314),[51] we defined active SEs (SE) using the active histone mark H3K27ac with the ROSE (Rank Ordering of SEs) algorithm.[54] We distinguished typical enhancers from active SEs using the ChromHMM-defined enhancer states and our previously published ROSE parameters.[104] All analyses were undertaken using the R platform for statistical computing (version 4.1 or later) using library packages implemented in *Bioconductor* or using the indicated software packages implemented in Java>1.6 and Python3.

Motif analysis

Known and *de novo* transcription factor motif enrichment was performed using *HOMER* v4.11 software utilizing the *findMotifsGenome.pl* command using default parameters. All analyses were undertaken using the R platform for statistical computing (version 4.1 or later) using library packages implemented in *Bioconductor* or using the indicated software packages implemented in Java>1.6 and Python3.

Quantitative real-time PCR

Total cellular RNA was isolated using the PureLink RNA Mini kit with on-column DNase treatment (ThermoFisher Scientific, Waltham, MA, USA). cDNA was prepared using the High-Capacity cDNA Reverse Transcription kit (Thermo Fisher Scientific). Quantitative real time PCR was performed on a QS6 Fast Real-Time PCR machine (Thermo Fisher Scientific) using Power Up SYBR Green Master Mix (Thermo Fisher Scientific) using the following human site-specific primers listed below. Data were analyzed using the QuantStudio Real-Time PCR Software (Thermo Fisher Scientific).

MYCN FWD: 5′ CACAAGGCCCTCAGTACCTC 3′
MYCN REV: 5′ ACCACGTCGATTTCTTCCTC 3′
RPS20 FWD: 5′ AAGGATACCGGAAAAACACCC 3′
RPS20 REV: 5′ TTTACGTTGCGGCTTGTTAGG 3′

Colony formation assays

Cells (500/well) were seeded in 6-well plates in triplicate in 2 mL of media. Media was replenished with or without indicated drug treatments every 2–3 days. After 3–4 weeks, cells were fixed and stained with 0.5% methylene blue in a 1:1 methanol: water solution and imaged once dry.

Invasion assays

Invasion assays were performed as previously described.[106] Briefly cells were harvest by trypsinization and resuspended in serum-free media. 1×10^5 cells were seeded into the top compartment of 8.0 μ m Biocoat Matrigel-coated invasion chambers (Corning, Corning, NY, USA) in duplicates. Complete media with 10% FBS was used as a chemoattractant in the bottom compartment. Cells were incubated at 37°C for 24hrs and bottom membranes were fixed and stained with the Hema3 kit (Fisher Scientific) according to the manufacturer's protocol. Cells were counted from 5 different view-fields per transwell.

Immunoblotting

Whole cell extracts were prepared in RIPA buffer (50 mM Tris-HCl, 150 mM NaCl, 1% Triton X-100, 0.5% sodium deoxycholate, 0.1% sodium dodecyl sulfate (SDS), 10% glycerol, 2 mM EDTA). Samples were resolved on 10% polyacrylamide gels and transferred to nitrocellulose membranes (Biorad, Hercules, CA, USA). Membranes were incubated overnight at 4°C with primary antibody diluted in blocking buffer. Appropriate HRP-conjugated secondary antibodies (Bio-Rad, Hercules, CA, USA) were used at 1:5,000 dilution in blocking buffer for 1 h at RT. Signals were visualized with BioRad chemiluminescence reagents and a GeneGnome XRQ NPC system (Syngene, Frederick, MD, USA).

Neurite analysis

Cells were treated with the indicated drugs or transduced with the indicated vectors and images were acquired using a Nikon Eclipse Ts2 inverted microscope and NIS Elements software (Melville, NY, USA). Quantification of percentage of cells with neurites, average neurites per cell, and average neurite length was carried out using the NeuronJ plugin[107] of ImageJ (National Institutes of Health, Bethesda, MD, USA).

Immunohistochemistry staining

Tissues were fixed in 10% buffered formalin for 24 h prior to processing. Tissues were embedded in paraffin and sectioned at 5 microns. Slides were de-paraffinized in several baths of xylene and then rehydrated in graded alcohols followed by ddH$_2$O. Slides were incubated in 1x pH 6 citrate buffer (Invitrogen Cat #00–5000) for 20 min. Slides were incubated in 3% H$_2$O$_2$ for 15 min. To block non-specific binding, tissues were incubated with 10% normal goat serum for 10 min, followed by avidin/biotin block (Vector Labs, Newark, CA, USA; Cat#SP-2001). Primary antibodies b3-Tubulin (1:400) from Cell Signaling Cat#5568, and N-Myc (1:800) from Cell Signaling Cat#51705 were diluted in 1% BSA solution and incubated for 30 min at room temperature, followed by the biotinylated Goat anti Rabbit secondary antibody (Vector Labs #BA-1000) for 15 min. For signal enhancement, ABC reagent (Vector Labs Cat #PK 6100) was applied for 30 min. To reveal endogenous peroxidase activity, slides were incubated with DAB substrate (Dako Cat #K3467) for 5 min and then counterstained with DAKO Hematoxylin for 20 s. Slides were dehydrated through several baths of graded alcohols and xylenes and then coverslipped. Images were acquired on a Leica Biosystem microscope with a 20X lens and a Flexacam C1 camera. Signal quantification was performed with ImageJ.

QUANTIFICATION AND STATISTICAL ANALYSIS

Experiments were repeated at least three independent times (exact n is indicated in figure legends). Statistical analysis was performed using Student's *t* test within Prism version 9 software (GraphPad, San Diego, CA), unless otherwise noted. A two-tailed p value < 0.05 was considered statistically significant for analyses. For mouse studies, the log tumor sizes were modeled as a function of treatment group, time, their two-way interaction, and random mouse effects using a linear mixed model. Tumor growth rates were compared between treatment groups using tests about the appropriate contrasts of model estimates. All model assumptions were verified graphically and all analyses were performed in SAS v9.4 (Cary, NC) at a significance level of 0.05.